CRANFIELD UNIVERSITY

PANAGIOTA CHATZI

CONDUCTIVITY GRADING IN EPOXY GRAPHENE OXIDE COMPOSITES USING THERMAL REDUCTION

SCHOOL OF APPLIED SCIENCES

MSc by Research
Academic Year: 2013 - 2014

Supervisor: Dr A. A. Skordos
February 2014

CRANFIELD UNIVERSITY

SCHOOL OF APPLIED SCIENCES

MSc by Research

Academic Year 2013 - 2014

PANAGIOTA CHATZI

CONDUCTIVITY GRADING IN EPOXY GRAPHENE OXIDE COMPOSITES USING THERMAL REDUCTION

Supervisor: Dr A. A. Skordos

February 2014

ABSTRACT

The aim of this project is the development of a method for the production of conductivity graded polymeric materials through the in-situ reduction of Graphene Oxide (GO). These types of composites can be used for the reduction of electrical field concentrations observed in several applications, such as cables, cable joints, microelectronic components and bushings. The evolution of electrical conductivity of GO was monitored during thermal reduction under isothermal and dynamic heating thermal conditions and compared with the kinetics of the reduction reaction as observed using calorimetry. These results were replicated in epoxy/GO composite to prove the feasibility of in-situ reduction and capabilities for controlling this process. In addition, reduction was achieved in epoxy/GO composites using infrared continuous and pulsed laser. It was shown that thermal reduction is possible in the cured epoxy composite at relatively low temperatures up to 260^{o}C. The kinetics of reduction follows a double mechanism which can be represented using a double n-th order process. Electrical measurements showed that conductivity increased significantly up to 0.12 S/m for dry particles and 0.09 S/m for the composite. Heat transfer by conduction and irradiation on specific areas resulted in selective reduction, and a conductive graded material.

Keywords: Graphene oxide, thermal reduction, electrical conductivity, epoxy resin, composites, laser treatment

ACKNOWLEDGEMENTS

I would like to express my sincere gratitude to my supervisor Dr Alex Skordos for his guidance, dedication and patience throughout this research project and for the opportunity he gave me to join the Composites Research group.

I would like to acknowledge ABB Switzerland Ltd that sponsored the project and especially Dr Emmanuel Logakis for his continuous support.

I am grateful to my supervisor Professor Stewart Williams and Dr Suder Wojciech for their help and excellent collaboration.

My truly thanks to Jim Hurley, Andew Dyer, David Ayre and Antonio Querreiro for their kindness, assistance and availability.

I am thankful to Elisabete Costa for her valuable help in the laboratory and her warm friendship.

I would like to thank all my colleagues and my friends who made Cranfield a pleasant place to stay.

I am deeply grateful to my parents and sister for their unending patience and sacrifice throughout my life which has given me the motivation and strength to work hard. Finally, I would like to thank Nikos for everything.

TABLE OF CONTENTS

LIST OF FIGURES

LIST OF TABLES

LIST OF EQUATIONS

LIST OF ABBREVIATIONS

CCG	Chemically converted graphene
CNT	Carbon Nanotube
CVD	Chemical Vapour Deposition
DMA	Dimethylacetamide
DMF	Dimethylformamide
DSC	Differential Scanning Calorimetry
FTIR	Fourier Transform Infrared Spectroscopy
GO	Graphene Oxide
MDSC	Modulated Differential Scanning Calorimetry
NMP	n-methylpyrrolidone
PC	Polycarbonate
PDMS	polydimethyl siloxane
PEGDA	polyethylene glycol diacrylate
PLA	Polyactic acide
PMMA	poly(methyl methacrylate
PVDF	polyvinylidene fluoride
PVOH	Polyvinyl alcohol
PVP	Poly vinylpyrrolidone
PVP/Vac	Poly (vinylpyrrolidone/vinyl acetate)
rGO	Reduced Graphene Oxide
TGA	Thermogravimetric Analysis
UV	Ultraviolet
XPS	X-Ray Photoelectron Spectroscopy

1 Introduction

1.1 Scope

The development of composites of carbon nanoparticles and polymers in recent years has resulted in materials with enhanced mechanical and electrical properties. Epoxy resins are widely used thermosets, with applications in the aerospace, marine, defence and electrical engineering sectors in modified forms with fibres or fillers. Fibres such as glass and carbon offer exceptional mechanical properties. Glass reinforced composites are used in relatively high strength applications that also require insulating properties. Carbon fibre composites offer high strength at a low weight and dominate aerospace applications. The high strength of these composites is combined with good electrical and thermal properties in the fibre direction [1]. Reinforcement with nanofillers can provide multifunctionality and improved properties in all directions. Carbon black has been used widely for applications requiring high electrical conductivity such as electrostatic discharge compounds, high performance coatings and automotive. Carbon nanotubes (CNTs) offer exceptional electrical properties at very low loading. This is combined with high elastic modulus and tensile strength; up to 1.25 GPa and 150 GPa respectively [2]. Incorporation of CNTs, GO and graphene in polymers is considered highly efficient due to the high aspect ratio of these nanoparticles.

As a one atom thick layer material, graphene has a two-dimensional structure consisting of sp^2-bonded carbon atoms arranged in a honeycomb lattice. Graphene holds great promise for many applications, such as nano-electronics, sensors, composites, batteries, supercapacitors and hydrogen storage due to its high surface area which increases capacitance. Recently a number of physical and chemical methods have been developed for the high yield preparation of graphene, notably chemical vapour deposition (CVD) [3], micromechanical exfoliation of graphite [4], epitaxial growth on an electrically insulating surface [5], and reduction. Mechanical exfoliation, which can achieve

uniform layers of graphene, is considered unsuitable for mass production. On the other hand, chemical exfoliation and epitaxial growth are appropriate for mass production, but they have limitations in terms of manufacturing cost and quality of graphene structure.

Graphene Oxide (GO) reduction is an alternative route for bulk production of graphene-based materials. GO is an intermediate product during the preparation of graphene. Although it is used to synthesise graphene, its advantage is that its electronic properties can be controlled by selective reduction [6]. GO is produced mainly by chemical exfoliation of graphite by intercalation (Hummers method) [7]. This method can produce GO in large quantities from inexpensive graphite powder as raw material. The reduction of GO can be achieved by chemical as well as thermal methods. Chemical methods use strong reducing agents such as hydrazine [8; 9], hydroquinone, alkaline environment or $NaBH_4$. Alcohols are believed to be effective reductants as they contribute to restoration of the graphite structure, fostering oxygen removal [10]. The most common drawback of chemical techniques is the generation of by-products. Thermal treatment is more attractive as it prevents defects by controlling the temperature. A low rate of temperature increase, can reduce the defects which are caused by a sharper temperature change. The combination of chemical techniques assisted by thermal reduction can lead to further deoxygenation without the need for high temperatures.

The electrical behaviour of GO based polymer composites can be modified using thermal reduction, converting the material form an insulator to a conductor. The idea of using GO as a filler instead of graphene is attractive due to its low cost and inexpensive production. Additionally, the presence of oxygen functional groups makes its dispersion in solvents and polymers easier and result in a stronger interface between the GO and epoxy. These unique properties have attracted interest for multiple industrial applications. The controllable electrical conductivity can provide electromagnetic interference shielding and contribute to lightning strike protection on the outer skin of aircraft creating when required, a conductive pathway and dissipating high currents. In

addition, GO based composites can offer reduction of electric field concentration. Elimination of field concentrations is of high importance as it often governs electrical performance.

Before using GO in technological applications, it is vital to understand its atomic structure as well as its behaviour in terms of reduction kinetics. Graphite oxide is formed by strong oxidation of graphite. Natural graphite flakes consist of many layers of graphene layers stuck together. The thickness of graphite flakes increases during oxidation due to the formation of oxygen groups. Several functionalisation types are introduced between the molecules, expanding the interlayer distance from 0.335 nm in graphite [11] and breaking the stacking between graphene sheets [12]. As an inhomogeneous and nonstoichiometric material, GO has a structure that is still elusive. Its chemical composition depends on its specific synthesis conditions. Several methods have been developed by Hofmann, Ruessin, and Scholz and Boem [13] in order to analyse the structure of GO. XPS results have shown that 59% of GO refers to graphitic groups, 29% corresponds to C-O bonds and 11.5% to C=O bonds [14]. The basis for the structure of the GO lies in the oxygen-containing groups and their arrangement through the carbon network. These oxygen containing groups are considered to be epoxides or hydroxyls across the carbon plane. Today the most widely accepted model is Lerf's [15], which proposes that epoxy and hydroxyl functional groups occupy the basal plane, and carbonyls, lactones and carboxyls are attached to the edges (Figure 1-1). This kind of structure disrupts the sp^2 hybridization resulting in a sp^3 network which prevents the conductive behaviour. Graphene exhibits high electrical conductivity in the horizontal direction along the layer. The presence of oxygen containing groups disturbs the planar structure and the electron transport, and induces high electrical resistivity of [16]. Consequently, deoxygenation could introduce the recovery of the GO conductivity [17]. The other functional groups attached to the edges have less influence in the electrical conductivity. As a result, the reduction of GO should mostly focus on the elimination of the epoxy and hydroxyl groups on the plane.

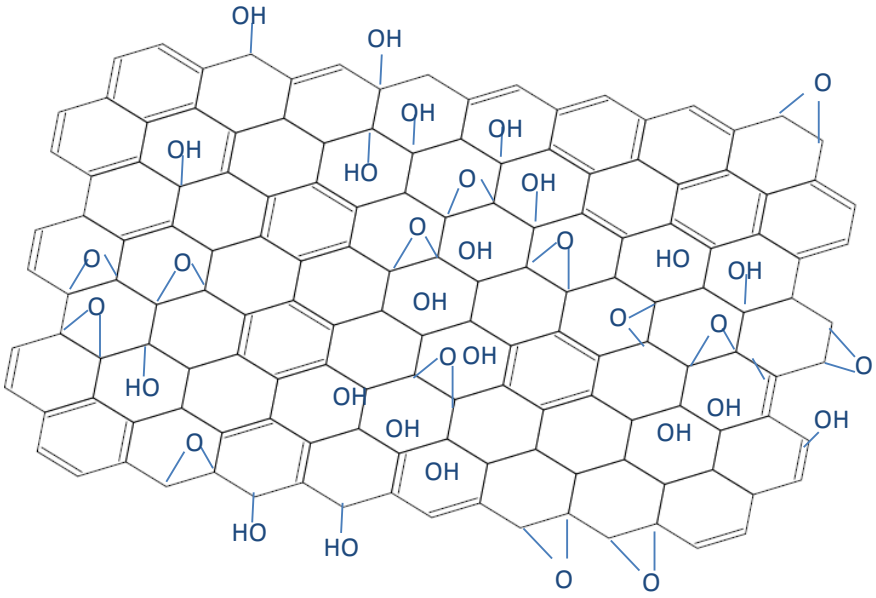

Figure 1-1 Structure of GO according to Lerf's model [15].

1.2 Motivation

Several researchers have studied the incorporation of GO in various polymers during the last decade. Most of the works focused on polar, viscous materials as well as polymers soluble in water [18-21]. Polarity ensures a high level of dispersion, and high viscosity prevents the re-aggregation of the particles. Thus, less polar and low viscosity polymers have received little attention and therefore the effect of GO in these materials is still elusive and further study is required. Although epoxy is widespread in various applications, a limited number studies have been conducted on the electrical properties of GO based epoxy materials.

The development of a method for the production of conductivity grading polymeric materials can be potentially used for the reduction of electrical field concentration. The manipulation of electrical conductivity is critical for these applications and can be advantageous for high current dissipation.

1.3 Aim and objectives

The aim of this project is to develop a method for the production of conductivity graded polymeric materials. Implementation of this concept is carried out by the

radiation induced reduction of epoxy/GO composites. To achieve this, the following objectives have to be met:

- Investigation of thermal reduction of GO.
- Fabrication of GO based composite.
- In-situ measurement of electrical conductivity during thermal reduction of GO inside epoxy.
- In-situ thermal reduction of GO in epoxy by irradiation.
- Evaluation of the selective reduction through electrical conductivity measurements.

1.4 Structure of the thesis

This thesis is organised in five chapters. This introduction presents the scope, the motivation and aims of the work. The literature review presents the current state of the art on thermal reduction of GO reduction and the in-situ reduction of the particles into polymers. The third part describes the materials used and explains in detail the fabrication methods, as well as the characterisation techniques. The fourth part reports and analyses the results. Conclusions and recommendations for further research are discussed in the final chapter.

2 Literature review

2.1 Introduction

2.2 Thermal reduction of GO

Many processes, such as mechanical exfoliation of graphite, CVD, chemical exfoliation and epitaxial growth, which are considered appropriate for production of graphene, have limitations in terms of production cost, quality of structure and production rate [22]. Chemical reduction of graphite oxide can cause the presence of contaminants which are responsible for poor electrical properties of the reduced GO (rGO). Currently, thermal methods can remove the oxygen to the extent permitted by the technique, the conditions and the temperature. Combination of thermal and chemical techniques improves GO reduction, [23].

2.2.1 Factors affecting thermal reduction

A significant advantage of thermal reduction is the possibility to control the reduction degree by altering the temperature, the duration of the process and the gaseous environment [23]. The degree of oxygen removal depends on heating rate, temperature and time [24; 25] whilst the kinetics of the process are reflected in changes in the electrical resistivity [26]. For example, the quantity of carbonyl groups after heating treatment at 150°C for 5 min is much lower than for heating treatment at the same temperature for 1 hour [27], which results in a much lower electrical conductivity.

The level of oxidation is found to be related to the temperature dependent electrical properties of rGO [28; 29]. Decreasing oxygen content, GO is submitted to a transition from a high resistivity to a low resistivity material following ohmic behaviour [30]. For instance, the reduction at temperatures of 500, 700, and 1000°C leads to conductivities of 50, 100 and 550 S/cm respectively [31], while treatment under N_2 flow leads to a conductivity of 8100 S/m at 700°C [32], and 1300 S/m at 220°C [33]. For a single layer of GO heated at a constant temperature of 200°C, the reaction order is expected to be 2.2 [26]. The heating of GO can be carried out under various atmospheres (high vacuum, H_2, Ar, N_2, NH_3 [32; 34-40]) which are required for the protection of the

system at high temperatures. For example, thermal reduction under H_2 flow is sufficient to remove the oxygen functionalities and restore the sp^2 carbon network while Ar_2 restores the sp^2 system but does not lower sufficiently the oxygen functionalities [32]. As a hydrophilic material, GO has residual H_2O which has to be eliminated before reduction. The drying temperature ranges from 50 to 100°C [25; 41-43] and its duration can be several hours.

2.2.2 Mechanism of thermal reduction

The deoxygenation mechanism is common for all reduction methods [22]. Thermal reduction is effective enough to eliminate oxygen groups but it has limitations regarding the production of high quality graphene. This is due to the presence of stable carbonyl and ether groups and formation of etch holes, which cannot be removed at temperatures lower than 600°C. These groups may cause damage to the C=C sp^2 bond network. Thermal reduction permits reactions of oxygen groups producing gas molecules such as H_2O, CO_2 and CO [25; 44; 45]. The desorption peaks of these gas molecules are observed at the same temperature [26]. However the complete mechanism of CO_2 and CO formation has not been elucidated yet. Epoxy and hydroxyl groups are considered to be detached from the graphitic plane, while highly unstable carboxyl groups can be eliminated at around 150°C from the plane [8; 23; 33] and at 400°C from the edges after thermal treatment [46].

X-ray Photoelectron Spectroscopy has indicated that epoxy groups are more stable than hydroxyl groups. These groups are attached to either the interior, or to the edge of an aromatic domain of GO. The interior groups tend to dissociate or migrate to the edges of aromatic domains. The hydroxyl groups can be fully eliminated and subtracted from the edges of GO only above 650°C [8]. However, a temperature increase even up to 150°C could enhance this mechanism. A second temperature range, proposed for the removal of the other functional groups, is at around 600°C, where the C/O ratio is increased to more than 13 [47]. Effective ways for the removal of the stable carbonyl and ether groups are the use of strong reductants as catalysts [41] and a temperature increase. During the process of thermal reduction, hydrogen atoms disconnect

from hydroxyls and connect with other neighbouring hydroxyls forming water molecules.

Figure 2-1 illustrates a schematic representation of the reduction mechanism. The two step reduction process followed by thermal treatment is an effective method to convert the sheets into reduced GO. Chemically converted graphene (CCG) is shown at steps 1, 2 and 3, some of the planar groups migrate to the edges and others react with NaBH (step 1) Groups such as hydroxyls completely leave the plane at 180°C (step 2) and the graphene structure is nearly restored in step 3 after annealing at 1100°C [48].

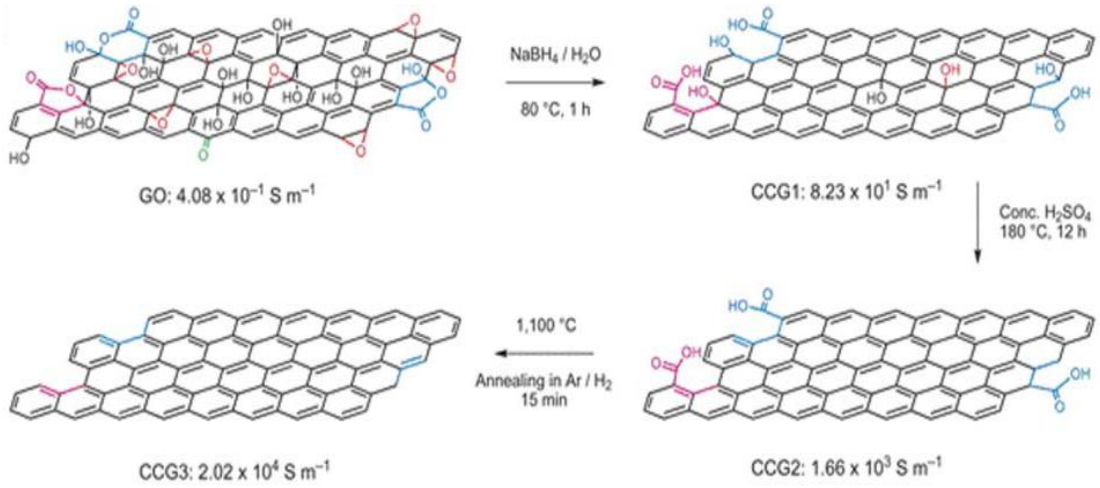

Figure 2-1 Schematic representation of GO reduction [48].

There are still open questions regarding the exact mechanism of reduction concerning the restoration of defects in the lattice during oxidation, or the amount of the remaining functional groups attached to the lattice, possibly because of the amorphous nature of rGO. Experimental work has shown that thermally induced reduction can remove a large number of functional groups at moderate heating for a few hours. However, the remaining amount of oxygen after annealing at 850°C is attributed to the formation of additional carbonyls at intermediate temperature [49]. Small quantities of oxygen are still present even at temperatures as high as 1100°C [46; 50] due to the further formation of carbonyls and epoxies from thermally dissociated hydrogen atoms [49].

Consequently, thermal reduction without the combination with chemical reduction cannot eliminate fully the oxygen content of GO [51].

2.2.3 Reduction at intermediate temperatures

Mild thermal reduction is a key challenge since it can be used as a method for the in situ reduction of GO inside polymers. Most thermosetting materials have a temperature limit, as their degradation happens at temperatures lower than 300°C. Reducing GO at high temperatures may efficiently remove most of the oxygen groups but introduces defects in the structure [30; 33; 52]. Existing approaches include thermal reduction at moderate temperatures with the presence of nanoparticles, chemical reducing agents, as well as solvo-thermal reduction in which the chemical-free thermal reduction occurs in GO dispersed in solvents.

Catalysts and reducing agents can be used to enhance reduction. Anhydrous $AlCl_3$ and Borohydride ($NaBH_4$) acting as a catalyst and reducing agent respectively can increase the reducibility of GO, enabling an electrical conductivity of 620 S/m and C/O atom ratio of 5.6 to be achieved at 150°C [41]. GO can be thermally reduced in various solvents such as ethylene glycol [39], water and DMA under atmospheric conditions [34], butanol and ethanol in the temperature range from 120°C to 200°C reaching C/O ratio of 5 [53]. DMF is considered to be more effective for reduction than water [54].

Dispersion under pressure facilitates reduction of GO in water up to 180°C [55], and in propylene carbonate at 150°C [35]. Thermal reduction of GO in ethanol can restore the sp^2 conjugation as ethanol intercalates into GO interlayers, contributing to the creation of new hexagonal carbon rings and preventing defect propagation [10]. Reduction under mild thermal treatment at 120°C in the presence of nanoparticles such as platinum acetylacetonate leads to simultaneous reduction and exfoliation of GO [56].

2.2.4 Irradiation induced reduction

Microwaves can heat GO in a very short time at low temperature (165°C) increasing the conductivity of rGO by four orders of magnitude [52]. The

absorption of microwaves depends on the amount of oxygen in rGO. The oxygen in GO decreases microwave absorption and the unoxidised regions in GO act as absorbents of the microwave energy which is then diffused through the rest of the structure by conductive heat dissipation [42].

Photographic flash reduction is a clean quick method consuming less energy than conventional heating [57]. It can achieve an electrical conductivity of around 10 S/cm on layers of GO [22; 58]. Although flash reduction can be conducted in air, flow of N_2 or Ar can decrease the required flash energy. A low power flashes are more suitable for a uniform outcome, rather than high power flashes, which could cause cracks and wrinkles due to rapid degassing. Since GO is black, energy absorption due to flash reduction occurs on its surface. The amount of the absorption within 1 μm of the surface is approximately 63% in the visible range. In contrast to conventional heating, a great advantage of flash and laser induced reduction is that they allows patterning on GO film [24; 58-62]. This allows the fabrication of functional surfaces and devices.

Sunlight can also be used for irradiation induced reduction. Solar radiation causes heating on the surface of GO increasing the temperature up to 150-200°C [63]. It has been shown that photolysis occurs at light excitations energies higher than 3.2 eV [44]. High conductivities in GO can also be achieved by exposure to UV light. This technique can be conducted either in the liquid phase with the presence of reducing agents and photocatalysts or directly on the GO sheet [61; 62; 64]. The liquid suspension changes colour progressively from brown to black [64; 65]. Examining the UV absorption spectra of GO and rGO, the treated material exhibits higher absorbance and a red-shifted peak, in comparison with the unreduced material. The spectrum of absorption of GO and rGO shows that absorption occurs at ~ 230 nm and ~265 nm respectively regardless of the type of laser treatment. For instance, both types of 532 and 355 nm laser irradiation, show similar results in the spectrum of radiation absorbance of rGO. Increasing the time of laser exposure results in higher absorbance at 265 nm gets higher until the reduction is complete. As a

result, the level of reduction depends on time, background gas and laser power [62; 66].

Simulations of temperature dynamics indicate that the temperature during laser irradiation at 50 mW can rise up to 1400°C which is sufficient for the complete reduction of GO even without reducing agents [67]. The irradiated area absorbs the laser energy which is converted to local heat. Elevated surface temperatures and increased sheet thickness enhance laser absorption [60]. Most of the oxygen is removed giving a sheet resistance of ~54 kΩ/sq [68]. It is concluded that techniques such as UV light and solar irradiation power can reduce the GO, but excimer laser irradiation can produce graphene almost devoid of oxygen functionalities in a short time [65].

2.3 Electrical properties of reduced GO polymer composites

2.3.1 Processing of GO composites for electrical applications

Graphene oxide can be reduced either before the incorporation in the polymer or inside the polymer [69; 70] to obtain electrically conductive graphene-polymer composites. Two basic methods have been developed for the production of reduced graphene oxide (rGO) composites. In situ polymerization is used to intercalate the GO with hydrophilic or polar polymers by interposing the monomer between the layers keeping them separated [71]. Grafting uses functional groups of GO which participate in the polymerisation reaction and are incorporated in the polymers forming covalent bonds [72]. For example, GO reacts with isocyanate groups of the monomer in polyurethanes, and grafting with vinyl polymers enhances the decomposition of oxygen moieties of GO [73]. Moreover, GO interacts with epoxy resin, during curing, due to the incorporation of GO into the cross-linked network [20; 74-80]. Solution or melt processing results in the production of single layer graphene sheets polymers with the use of stabilisers and surfactants [21].

Fabrication of high quality GO based polymers requires the exfoliation of GO, before mixing with the polymer. Dispersion of GO particles is an important step in the process that governs the quality of the final material [81]. Carbon

nanofillers have a high surface area which promotes agglomeration and the creation of micro particles due to van der Waals interactions [21; 82; 83]. Agglomeration is more pronounced in cases of anisotropic particles such as GO, due to the high inter-particle interaction. As a result, efficient dispersion is necessary to exfoliate GO as it provides the best opportunity for bonding with the medium [84]. Solvent assisted dispersion is conducted by mechanical exfoliation, mainly ultrasonication and shear mixing [3]. The van der Waals forces between the layers can be counteracted by the energy of ultrasonication. Ultrasonication reduces agglomeration, increasing the distance between the layers and forming colloidal suspensions of GO [85]. However, it is not adequate for mass production because the vibrational energy attenuates as the distance from the ultrasonic source increases [86; 87]. Direct dispersion of GO powder in epoxy resin is not effective, due to the difficulty of ultrasonic energy transfer in such a viscous suspension.

The presence of functional groups makes GO hydrophilic, so it can be easily dispersed in aqueous media and polar solvents. Oxygen groups enhance the intercalation of water in graphite oxide interlayer positions [84]. Water molecules prevent agglomeration of GO sheets. The functional groups can contribute to dispersion as they can change the van der Waals interactions increasing dispersibility [70]. GO can be dispersed in many organic solvents such as acetone [87; 88], ethanol [85], dimethylformamide (DMF) [72; 81; 89-92], Propylene Carbonate [35] and n-methylpyrrolidone (NMP) [93-95] but it cannot be dispersed directly in non-polar organic solvents and polymers [50; 84].

Use of functionalised GO enhances dispersion in low polarity media. However, chemical functionalisation is costly and potentially hazardous [85]. Therefore, environmentally friendly methods which do not require organic solvents and chemical functionalisation have been developed based on the dispersion of GO in aqueous media and mixing with water soluble polymers [96; 97]. Gudarzi et al. [84] utilised dispersion of GO in water and functionalisation of GO using an aromatic diamine to ensure compatibility of GO with epoxy resin and high

dispersion. Colloidal polymer particles are used to incorporate GO into non water soluble polymers [98].

Graphite oxide is exfoliated into single layers of GO during dispersion. Exfoliated single layers of GO result in maximum enhancement of the properties of polymers [99]. Moreover, this structure allows easy removal of the oxygen groups during reduction. After the removal of most oxygen groups of single layers of GO and the restoration of the sp^2 bonds, the electrical conductivity is recovered. In the case of polymer composites, a special treatment has to be carried out during thermal reduction due to phenomenon of aggregation as rGO becomes less hydrophilic when the temperature rises [69; 87].

After the dispersion of GO in the solvent, the direct incorporation of colloidal suspensions of GO platelets in the polymer and the removal of solvent may cause aggregation of the platelets. Therefore, the GO solution has to be dissolved in the polymer by shear mixing or stirring [69]. Storage of the dispersed blend for long periods is not recommended since the platelets settle over time and potentially re-agglomerate. The GO suspension can remain stable at high pH for a long time unlike neutral and low pH suspensions [35]. The kinetics of re-agglomeration depends on the viscosity of the resin. Some limited reaction of the resin suspension with the hardener is proposed in order to prevent re-aggregation [72; 100].

Polar polymers have higher electrical conductivity. The electric behaviour of rGO based polymer composites can be affected by the content of rGO. Higher GO loading can allow the creation of a conductive network. However, the main goal is to keep the particle content as low as possible.

2.3.2 In-situ thermal reduction of GO in polymers

Successful strategies for the in situ thermal reduction of GO in polymer composites have been reported for a variety of polymer matrices. As GO particles tend to re-aggregate at high temperatures, the presence of polymers in solution during reduction can also prevent restacking of the sheets [101]. The electrical properties of GO composites can be manipulated by changing the

oxidation state. The oxidation state depends on the temperature of reduction and the duration of the process. For example, the resistivity of GO-PVDF composites gradually decreases with temperature, with a sharp decrease above the melting point of the composite [102]. The reduction of GO dispersed in poly(dimethyl siloxane) (PDMS) at several temperatures results in the increase of both dielectric constant and loss factor. In this case the material insulating properties are not completely eradicated after the reduction at 160°C [103] showing that above this temperature the GO deoxygenation becomes more efficient. GO can be reduced in polymers at temperatures as low as 200°C [72]. The reduction in polymers starts at about 150°C and is completed at about 250°C either under dynamic or isothermal conditions, with the contribution of additives at low temperatures for isothermal experiments [19; 81; 90; 92; 104; 105]. No significant change in weight loss and C/O ratio is detected above 250°C [106].

Graphene oxide reduction in polymers can be carried out using the same heating methods as for dry GO and GO in solvents. Apart from conventional heating, UV light and microwaves can be applied to the material for polymerisation and reduction [107; 108]. GO can be thermally reduced in Polyvinyl alcohol (PVOH) [19], polyvinylidene fluoride (PVDF) [72; 92], poly (vinylpyrrolidone) (PVP), poly (vinylpyrrolidone/vinyl acetate) (PVP/Vac) [90], poly(methyl methacrylate (PMMA)[108] and epoxy [109]. In-situ thermal reduction in PVDF can achieve electrical conductivity 3 orders of magnitude higher than the untreated material [72]. The reduction of GO in Polyamide-6, through in situ polymerisation of ε-caprolactam monomer results in enhanced electrical properties, a percolation threshold as low as 0.41 vol.% and conductivity of 0.028 S/m at 1.64 vol.% GO [104; 106]. The percolation threshold can reach 0.21 vol% after the in situ reduction of GO during the processing of polycarbonate (PC) [81], 3 wt% in polyethylene glycol diacrylate (PEGDA) [107] and 0.5 wt% in PVDF [92].

Table 2-1 summarises the electrical conductivity of composites after reduction and the corresponding GO loading. The percolation threshold varies depending

on the material. Reduction in PVDF increases the conductivity up to 10^{-4} S/m at a very low percolation threshold of 0.05%, while high loading of polyvinyl alcohol results in a conductivity reaching 4 10^{-2} S/m.

Table 2-1 Electrical properties of GO based polymers after in situ reduction ([a]converted from vol% to wt% using an average density of graphite (2000 kg m^{-3})), ([b]converted from the sheet resistance using sheet thickness 25 µm according to reference [19])

Type of polymer	Procedure	Percolation Threshold (wt%)	Filler content (wt%)	Conductivity achieved [S/m]	Reference
PVDF	In-situ thermal reduction	0.05[a]	0.05[a]	10^{-4}	[102]
Polyamide-6	In-situ thermal reduction during polymerisation	0.081[a]	3.23	0.028	[104]
Polycarbonate	In-situ thermal reduction during polymerisation	0.42[a]	2.16[a]	0.041	[81]
Polyethylene glycol diacrylate	In-situ thermal reduction during UV polymerisation	3			[107]
PVDF	In-situ thermal reduction during hot press moulding	0.5	1.5	10^{-5}	[92]
Epoxy	Thermochemical reduction during in situ polymerisation	0.8[a]			[110]
Polyvinyl alcohol	Thermochemical reduction	9.4	9.4	0.04[b]	[19]

In-situ thermal reduction of GO in polymer composites is often not sufficient for maximising electrical conductivity [111]. The low conductivity of 2.3 × 10^{-7} S/m of GO in polyactic acid (PLA) proves that its reduction is not sufficient [105]. Moreover, GO/polystyrene composites still retain their insulating properties after heating [112]. Well dispersed GO in polyimide matrix can be reduced after thermochemical treatment during imidisation [113] whereas, GO in epoxy and sulfonated tetrafluoroethylene (Nafion) results in good electrical properties (~1 S/m at 6 vol%) if the material undergoes heating in combination with exposure

to chemical substances like hydrazine [110], which boosts the GO decomposition especially if mild thermal treatment is needed [19; 108; 114].

3 Materials and methods

3.1 Raw materials

3.1.1 Epoxy system

The resin system used is the Araldite CY 221 epoxy and the hardener is the Aradur 2966 amine supplied by Huntsman. This system is suitable for encapsulating or potting of low voltage and electronic components. This low temperature curing matrix system has a low viscosity of 490 mPas at 25 °C and 205 mPas at 40°C. Its glass transition temperature (T_g) in the fully cured state is 25°C. At 40°C the gelation time is 45 min [115]. The recommended cure cycle is 24-48 hours at ambient temperature and 4 hours at room temperature and 4 hours at 60°C. The mixing ratio is 100 parts by weight of resin to 25 parts by weight of hardener [115].

3.1.2 Graphene oxide

Graphene oxide was supplied by Nanoinnova [116] in the form of powder. The nominal thickness of the GO flakes is between 0.7-1.2 nm. The grain size varies up to 100 µm. Elemental analysis shows that the material consists of 2.32% H, 0.04% N, 0.8% S and 0.05% Mn. The O/C atomic ratio is 0.655. GO paper was supplied by Graphene Laboratories [117]. GO paper was selected due to handling difficulties of powder in several experiments. The paper has a diameter of 4 cm, and a thickness of 10 µm. The O/C atomic ratio does not exceed 0.45 [117].

3.2 Preparation of GO/Epoxy composites

GO composites were prepared following the procedure summarised in Table 3–1. GO powder was dispersed in the resin using ultrasonication and high shear mixing. Composites were fabricated using casting and curing in a mould or curing on interdigitated sensors [118]. The final particle content in the epoxy system was 10 wt%. The initial dimensions of the composite samples which were cast and cured in the moulds were 90x90x0.5 mm.

A Branson 90 W digital sonifier with an ultrasonication horn was used for the processing of 16 mg/ml suspensions of GO. The device can be connected to a computer for energy and temperature recording. As a result, the progress of the process can be qualified through the evaluation of the energy emitted by the horn. The first step included ultra-sonication in acetone for 4 hours operating at 40% magnitude of power. In the second step, water was added and the acetone evaporated. The duration of ultrasonication in that step was 1 hour and the power increased to 60%. A temperature probe was put inside the liquid in order to control the maximum temperature and avoid overheating of the mixture. An ice bath maintained the temperature of the treated media below 30°C. Subsequently, the suspensions were mixed with the resin at 80°C, at 2000 rpm under vacuum until the evaporation of water (approximately 4 hours) using a VMA Dispermat shear mixer. A scale was used to check the level of water evaporation. It is assumed that a very small amount of water and aceton (~3 wt%) could not evaporate completely. The required amount of Aradur 2966 curing agent was added to the GO/Araldite resin mixture. The blends were stirred thoroughly making sure that the hardener was mixed with the resin. The GO/resin system was already degassed and no further degassing was necessary. The blends were poured into the mould which was made of two clamped square glass plates sandwiching silicone rubber at the edges, for the sealing of the system (Figure 3–1). Release agent had already been applied on each side of the glass plates. The system was cured for 4 h at ambient temperature and post-cured for 4 hours at 60°C in an oven according to the procedure recommended by the supplier [115]. In the case of samples cured on dielectric sensors [118], a layer of the composite, with a thickness of about 0.4 mm, was applied with a spatula on the top surface of the interdigitated grid. Figure 3–2 illustrates the sensor and its dimensions.

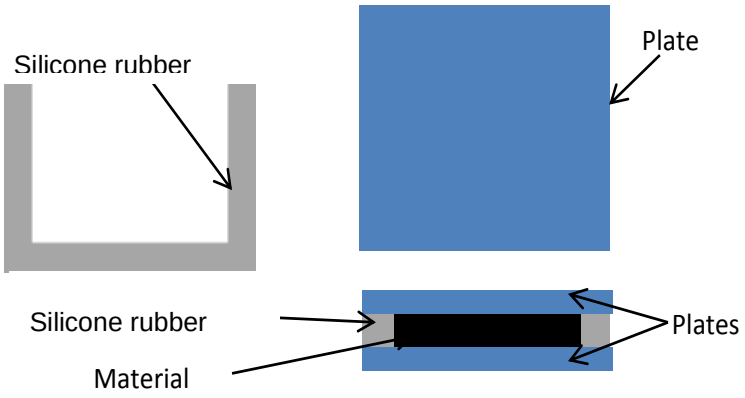

Figure 3-1 Mould used to cure the composites.

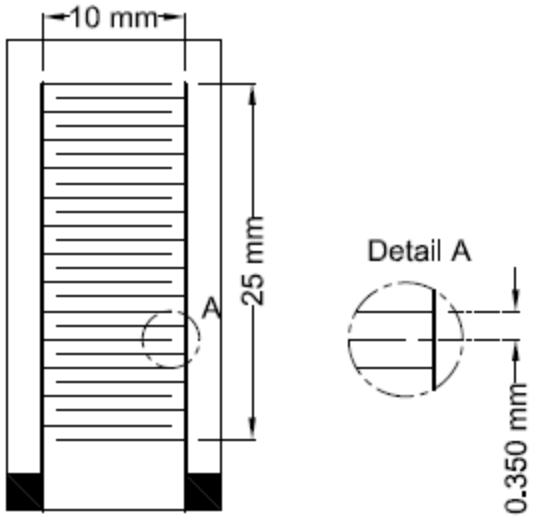

Figure 3-2 GIA dielectric sensor [118].

Table 3-1 Method of incorporation of GO into epoxy resin.

Step	Procedure
1	Ultra-sonication in acetone for 4 hours
2	Addition to water
3	Ultra-sonication in water for 1 hour
4	Addition of resin
5	High shear mixing under vacuum and evaporation of water
6	Addition of hardener
7	Hand mixing for 5 minutes
8	Casting and curing

3.3 Laser

Two different lasers were used for irradiating the samples: An Nd:YAG pulsed laser (model GSI JK 300HPS) with 300 W average power, operating at 1064 nm giving pulsed energy to the samples and a CW modulated fibre laser (model SP20P-0202) with 20 W output power heating the samples continuously. The continuous laser was operating in infrared wavelength. The configuration of the experiment is shown in Figure 3-3.

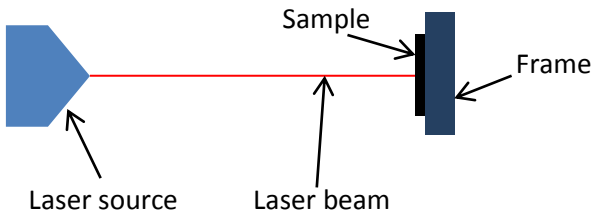

Figure 3-3 Schematic diagram of laser process for heating composite sample.

The samples of 10 wt% GO/epoxy with 0.5 mm thickness, were cut in dimensions of 20x20 mm. They were fixed onto a frame with tapes transparent to the laser adjusting it to the correct level for the laser beam. The peak and average power can be controlled by the operator changing the beam size, scanning speed, pulse duration, and frequency. The mean laser energy can be defined by calculating the area under the power curve (Figure 3–4).

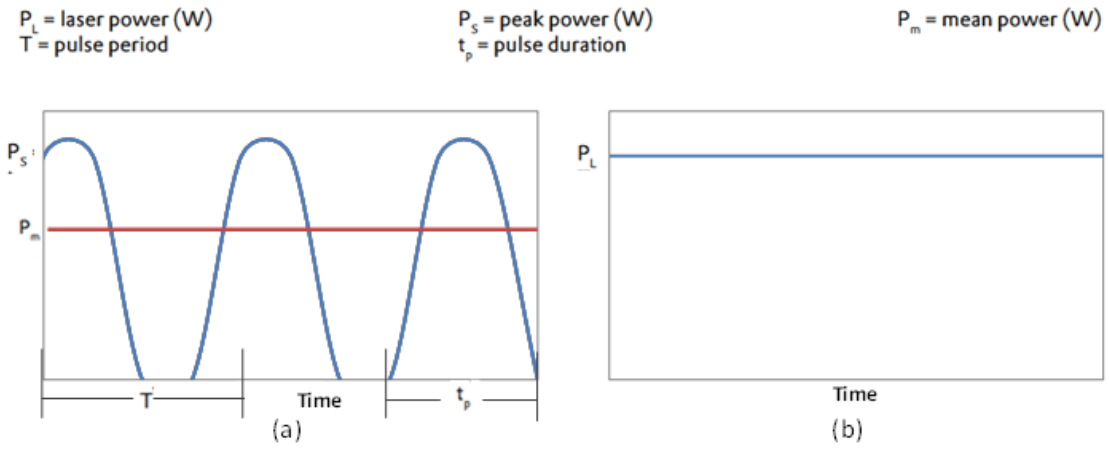

Figure 3-4 Power profiles in the types of laser used. a) Pulsed wave laser, b) Continuous wave laser.

The scanning speed was constant at 200 mm/min in all cases for both types of laser. The peak power depends on pulse duration for the pulse laser. The average power of the process is determined by the pulsed energy and its frequency. The laser beam size affects the amount of energy concentrated in that specific area. When the beam diameter increases, the energy is distributed over a larger area. The beam diameter varied from 5 to 10 mm for the pulsed laser and from 0.8 to 4 mm for the continuous laser. The various parameters which were applied for each laser are listed in Table 3-2.

Table 3-2 Parameters used for pulsed and continuous laser

Condition	Type	Beam diameter [mm]	speed [mm/min]	Pulse [ms]	Peak energy [J]	Frequency [Hz]	Track distance [mm]	Average power [W]
1	Pulsed	5	200	3	0.23	15	N/A	3.45
2	Pulsed	8	200	3	0.23	15	N/A	3.45
3	Pulsed	8	200	3	0.23	10	N/A	2.3
4	Pulsed	10	200	3	0.23	10	N/A	2.3
5	Pulsed	10	200	3	0.23	20	N/A	4.6
6	Pulsed	10	200	3	0.23	15	N/A	3.45
7	Pulsed	8	200	2	0.15	10	N/A	1.53
8	Pulsed	5	200	2	0.15	10	N/A	1.53
9	Pulsed	8	200	2.5	0.2	10	N/A	2
10	Pulsed	6	200	2.5	0.2	10	N/A	2
11	Continuous	0.8	200	N/A	N/A	N/A	1	1.155
12	Continuous	0.8	200	N/A	N/A	N/A	1	0.636
13	Continuous	0.8	200	N/A	N/A	N/A	0.7	0.809
14	Continuous	0.8	200	N/A	N/A	N/A	0.7	0.636
15	Continuous	4	200	N/A	N/A	N/A	1	2.02
16	Continuous	4	200	N/A	N/A	N/A	1	2.995
17	Continuous	4	200	N/A	N/A	N/A	2	2.995
18	Continuous	4	200	N/A	N/A	N/A	1.5	2.995
19	Continuous	0.8	200	N/A	N/A	N/A	0.5	0.809
20	Continuous	0.8	200	N/A	N/A	N/A	0.5	0.982

3.4 Characterisation

3.4.1 Differential Scanning Calorimetry

Differential Scanning Calorimetry (DSC) experiments were performed on GO paper, GO powder and the GO based composite samples. Before every test of the two types of GO, the particles were dried at 95 °C for 4 hours to remove extra water that could affect the result due to evaporation. The DSC experiments were conducted under a nitrogen flow of 50 ml/min using a Q200 TA Instruments MDSC with a sample amount ranging from 2 to 5 mg.

Isothermal and dynamic thermal profiles were used. In isothermal experiments all samples were heated using a rate of 20°C/min up to the dwell temperature and then kept there for a pre-specified duration. Dynamic experiments included heating up to 260°C at several heating rates. Tables 3–4 and 3–5 summarise the conditions for each case.

Table 3-3 Temperature profiles of isothermal DSC tests.

Isothermal tests			
Case	Rate [°C/min]	Target temperature [°C]	Duration [min]
1	20	160	300 (dry GO), 840 (composite)
2	20	180	120 (dry GO), 720 (composite)
3	20	200	120
4	20	220	60

Table 3-4 Temperature profiles of dynamic DSC tests.

Dynamic tests		
Case	Rate [°C/min]	Target temperature [°C]
1	5	260
2	1	260

The total enthalpy was calculated by the integral under the DSC curve. The baseline was different between isothermal and dynamic tests. The type of baseline for the dynamic heating was tangential sigmoidal. For this baseline four points were selected, two at the beginning of the curve and two at the end. The baseline was tangent at the two set of points which were the limits of integration. A horizontal baseline was used for the integration of the isothermal runs. The level of the horizontal baseline was defined by the level of the DSC signal plateau at the end of the experiment. The starting point was defined by the time at which the temperature reaches its dwell value.

3.4.2 Thermogravimetric Analysis

Thermogravimetric analysis (TGA) was carried out using a Q500 TGA (TA Instruments). The tests were conducted in a controlled atmosphere of nitrogen flow, to control the reduction process and protect the system from corrosive and oxidising gases. The measurements were carried out isothermally at 200°C and dynamically with a ramp rate of 5°C/min up to 260°C for GO powder, paper and GO composite samples. Additionally, a test was carried out for the GO composite and neat resin to check the temperature of degradation. The test included heating up to 500°C using a ramp rate of 5°C/min.

3.4.3 Fourier Transform Infrared Spectroscopy

Fourier transform infrared spectroscopy (FTIR) measured the transmission in GO samples in the wavelength range of 400-4000 cm^{-1} at ambient temperature. The apparatus included an infrared source, an interferometer to isolate the frequencies and a detector to measure the intensity of the radiation at each frequency. The spectrometer was a Thermo Nicolet Avatar-370 (Thermo Electron Corporation). Before the tests, the samples were heated dynamically under nitrogen flow. The level of reduction was investigated after reaching the temperatures of 150, 180, 200 and 220°C using a ramp rate of 5 °C/min. After heating, the samples were mixed with KBr dried for 10 minutes at 60°C to remove water and pressed together to form a compact disc.

3.4.4 Transmission Optical Microscope

The morphology of the suspensions was investigated with an optical microscope in transmission mode. An Olympus BH-2 microscope was utilised to acquire images of the samples using transmitted light to evaluate the level of dispersion as well as the particle size of GO inside the liquid. One droplet of the suspension was deposited on a glass slide and covered by a coverslip. The dispersion state was evaluated using microscopy at the end of steps 1, 3, 5, 7 of Table 3-1. Particularly, if the size of the particles was less than 10 μm at the end of the process, the dispersion method was considered successful.

3.4.5 Stereo Microscope

The surface of composite samples was examined through stereo microscopy. The microscope is a Nikon SMZ-2T stereo zoom, fitted with a JVC KY-F55B colour camera.

3.4.6 Impedance Spectroscopy

AC spectroscopy measurements were carried out using an Impedance Analyser Solatron SI 1260 over the frequency range from 1 Hz to 1 MHz. Twenty five frequencies were swept in a logarithmic scale at specific time intervals during the experiment. The results were acquired in the form of capacitance and resistance corresponding to a parallel RC circuit. A piece of GO paper in 5 mm diameter was placed between parallel copper discs of the same size (Figure 3–5) and an AC voltage of 1 V amplitude was applied. The copper discs were connected to the analyser for the AC measurements. The electrical conductivity of GO paper was calculated using the real impedance obtained and the geometry of the sample. It is assumed that the GO paper was in intimate contact with the copper discs over the complete area, so that the current flow was uniform over the entire area.

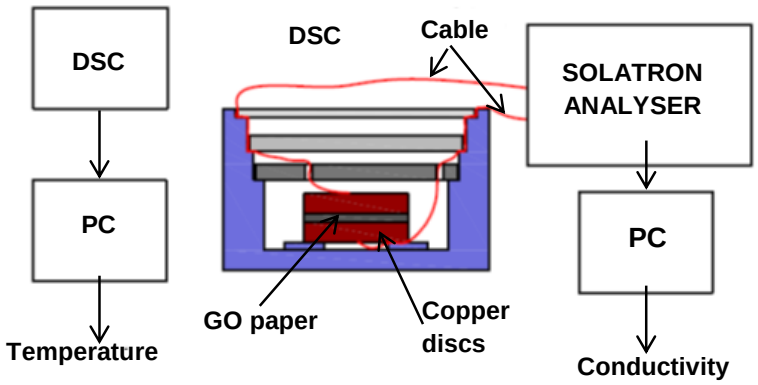

Figure 3-5 Schematic of the setup used for the conductivity measurements.

In the case of GO/epoxy composite samples a small amount of the material was deposited on an interdigitated sensor (GIA) connected to the frequency analyser. Two calibration formulas were used for determining the permittivity and the dielectric loss of the material [119; 120]:

$$\varepsilon' = 3.93\frac{C_s}{C_0} - 2.93 \quad (1)$$

$$\varepsilon'' = \frac{3.93}{2\pi f C_0 R} \quad (2)$$

where C_s, C_0, R, and f, are the measured capacitance, the air capacitance of the sensor, the measured resistance and the frequency respectively. The results were translated to the real part of complex conductivity (σ') as follows:

$$\sigma' = 2\pi f \varepsilon'' \varepsilon_0 \quad (3)$$

The samples were put inside a DSC cell in order to be heated under nitrogen flow, to ensure that the copper discs were free of oxide, and the temperature was recorded. Two insulated wires were connected to the copper discs in the case of the GO paper and to the GIA sensor terminals in the case of the composite. It should be noted that the soldering pads of the sensor are are at distance from the electrode in contact with the composite ensuring that the state of the material is not altered during soldering. This setup allowed the in situ conductivity measurement of GO during thermal reduction in the composite. The thermal profiles in these tests are described in Tables 3-5 and 3-6. The samples of GO paper were dried at 95 °C for 4 hours before the tests.

Table 3-5 Temperature profiles of isothermal impedance spectroscopy tests

Isothermal tests				
Case	Rate [5°C/min]	Target temperature [°C]	Duration [min]	
			GO paper	**Composite**
1	20	160	1440	1440
2	20	180	900	900
3	20	200	720	720
4	20	220	290	300

Table 3-6 Temperature profiles of dynamic impedance spectroscopy tests

Dynamic tests		
Case	Rate [5°C/min]	Target temperature [°C]
1	5	260
2	1	260
3	0.2	260

3.5 Measurements for conductivity grading of the GO based composite

Conductivity measurements were conducted on a composite rod with length 45 cm and diameter 8 mm in order to investigate the grading of conductivity. The electrical measurements were carried out using the solatron impedance analyser connected to an interdigitated sensor surrounding the sample at 9 different points through the length and at diametrical positions across the circumference. As perfect contact between the sensors and the rod could not achieved, 18 records were obtained several times and the average conductivity was calculated at each location taking into account equations (1)-(3). A thermal gradient was imposed on the sample using a cylindrical copper heating element which was in local contact with the sample. A Eurotherm 2408 PID temperature controller was used for the temperature programming and control. K-type thermocouples, immersed in the rod at 3 different positions along the lengh, were connected to a DAS-TC board. The programmed temperature was set at 220°C. After heating of the rod, the sample was cooled down to ambient temperature.

4 Results and discussion

4.1 Dispersion evaluation

Figure 4–1 illustrates the outcome of the dispersion process presented in paragraph 3.2. The presence of dark areas indicates the low level of exfoliation at initial steps of ultrasonication (30 and 90 min in acetone). These dark particles are thick flakes of agglomerated sheets. This morphology prevents the development of a percolating network. The dispersion state is improved after sonication in water due to the polar nature of the solvent. The mixture exhibits homogenous dispersion in the final step. The particles are small and there are not large aggregates. The average size of dispersed particles inside the resin was estimated to be about 10 μm. The average size of the original material was significantly greater than 50 μm. After curing, the particles size remained the same as the size after shear mixing in resin.

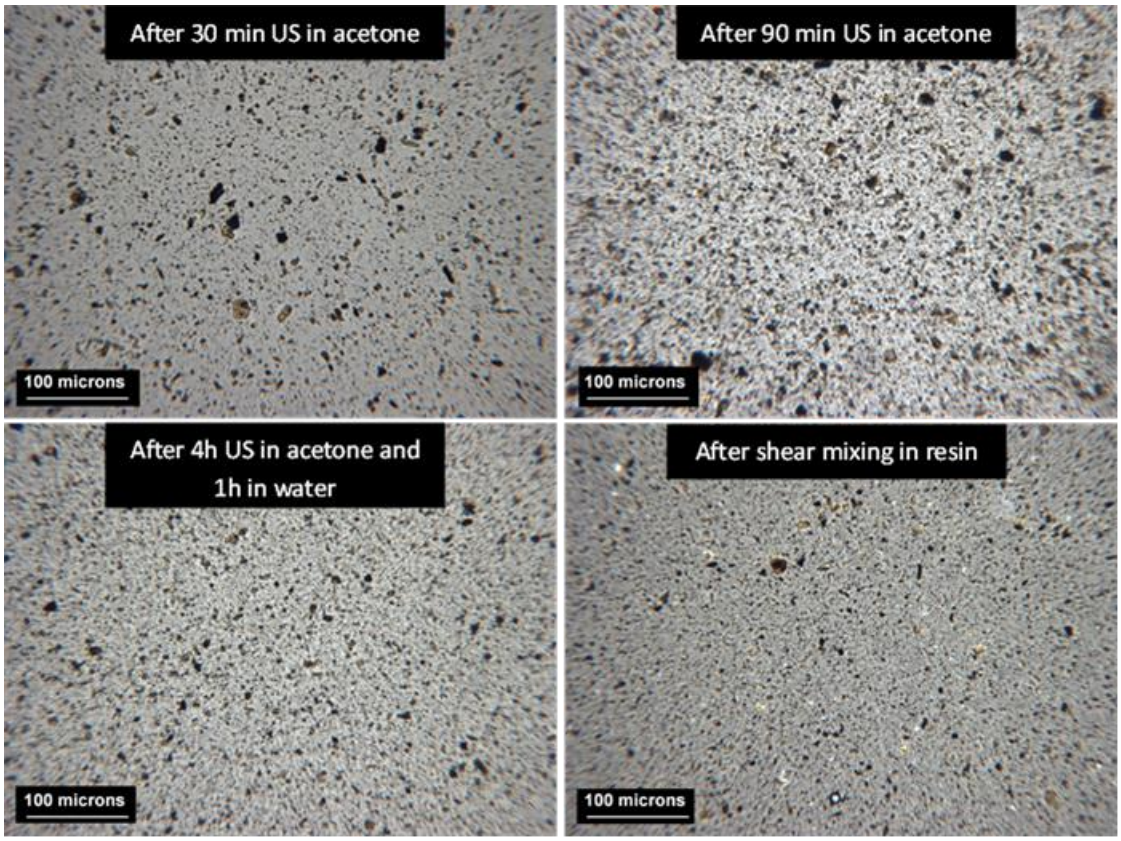

Figure 4-1 Transmission optical micrographs of GO suspension at various steps.

4.2 Evolution of thermal reduction

A series of experiments was carried out in order to investigate the occurrence and kinetics of GO reduction. In particular, DSC and TGA were used to determine the reduction kinetics and mass loss respectively. Dielectric spectroscopy was used to evaluate the evolution of electrical response during the reduction. The results were correlated to each other, to estimate the links between the electrical response and chemical reduction sate. FTIR was conducted to study the structure of GO. The study of correlation between the chemical kinetics and electrical conductivity was carried out for the dry GO particles and the GO/epoxy composite.

4.2.1 Investigation of chemical structure of GO and rGO

Figure 4-2 shows the evolution of FTIR spectra of rGO. The thermal treatment up to 150°C does not cause significant reduction at the heating rate used. The GO spectrum shows strong bands at 3420, 1720, and 1620 cm^{-1} which verify the presence of hydroxyl (-OH), carbonyl (C=O) and aromatics (C=C), respectively. The peak at 1390 cm^{-1} is attributed to the hydroxyl and carboxyl (C-O) acid groups. The C-O stretching vibrations at 1230 and 1050 cm^{-1} signify the presence of epoxy and alkoxy groups respectively, which are stable in these conditions. At 180°C the intensity is slightly reduced at 1720, 1620 and 1230 cm^{-1} and the other peaks remain unaffected. As the temperature reaches 220°C the absorption at 1390 cm^{-1} is totally eliminated, indicating that the functional groups of hydroxyl and unstable carboxyl are removed. This confirms that the decomposition of carboxyl groups starts at low temperatures [54]. Stable epoxies and hydroxyls are considered to be detached from the base plane and migrate to the edges of aromatic domains. The presence of the stable carbonyl and ether groups, which are found at 1720 and 1230 cm^{-1} respectively, cannot be removed at temperatures lower than 600°C [23]. As the reduction continues at higher temperatures, the peaks of the absorption of aromatics and carbonyl become weaker. However, the aromatic bonds are too strong to decompose even at high temperatures [121]. Additionally, the residual peak at 1720 cm^{-1} is attributed to the remaining carbonyl which is more stable. Furthermore,

disappearance of the peak at 1030 cm^{-1} occurs at 220 and 260°C which proves that more hydroxyls have been removed.

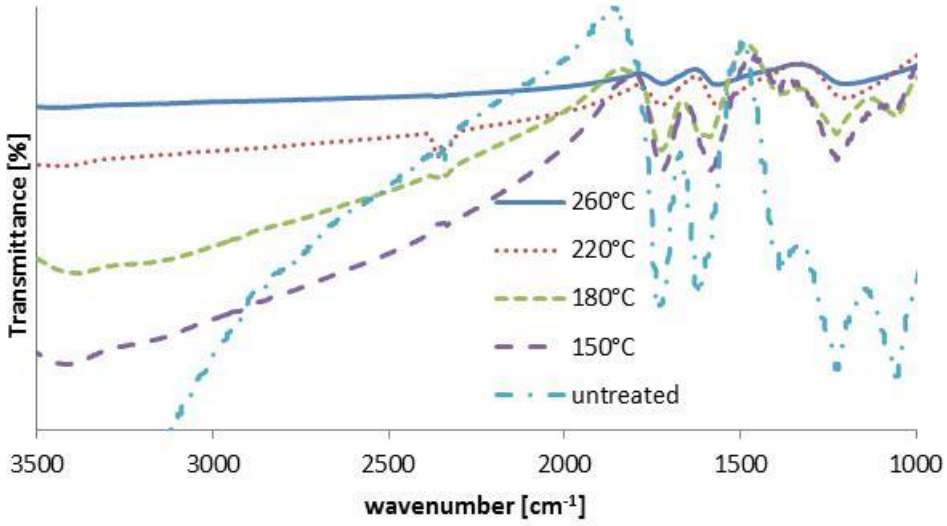

Figure 4-2 FTIR spectra for GO powder reduced at different temperatures.

4.2.2 Thermogravimetric Analysis

Figures 4-3 and 4-4 illustrate the weight loss during reduction of GO paper, GO powder, composite and neat epoxy heated at the rate of 5°C/min. The weight loss evolution is similar for the GO paper and powder. Nevertheless, the evolution of loss weigh follows different slope comparing the dynamic heating with the isothermal, as shown in Figures 4-3, 4-4. In Figure 4-3 there is a slight weigh reduction in paper and powder up to 100°C due to residual water evaporation. The weight loss is still insignificant in the temperature range from 100 to 170°C and only 5% due to the possible decomposition of unstable carboxyls. There is a substantial mass loss starting from 170°C which is completed at 220°C. In this region, where hydroxyls and carboxyls may be removed the weight loss is estimated to be about 30%. The reduction of GO in this step corresponds to oxygen release in the form of CO_2, H_2O, and CO. Over 220°C the GO decomposition may continue but no rapid weight loss is observed. In the GO/epoxy composite, the mass loss has a different evolution than in the dry GO. The reduction is manifested clearly only up to 200°C. The resin starts decomposing but the starting time is not clear. The inset in Figure 4-

3 shows the normalised curve according to the load of 10% GO in the pure reduction region up to 200°C. The normalised curve was calculated by dividing the total weight of the composite material with 10%, in order to obtain the pure weight of GO. The weight loss is massive in the reduction region, reaching 60%. This massive weight loss indicates significant gases release mostly in the temperature region from 140 to 180°C. The slight change of the slope in this region suggests the completion of reduction in two steps. Further weight loss occurs over above 220°C mainly due to thermal decomposition of the resin. The most thermally stable material up to 310°C is neat epoxy. The beginning of decomposition of the neat epoxy is found at 310°C where the weight loss is 70%. Below this temperature the slight weight loss of 10% indicates insignificant gases release which starts from 220°C. Thus, it can be concluded that the reduction of GO inside the epoxy continues above 220°C, and from 310°C two phenomena can take place: further reduction of GO and the decomposition of epoxy. It is clearly shown that the decomposition of the resin starts at lower temperatures than the neat epoxy. The complete decomposition of neat epoxy occurs over 400°C.

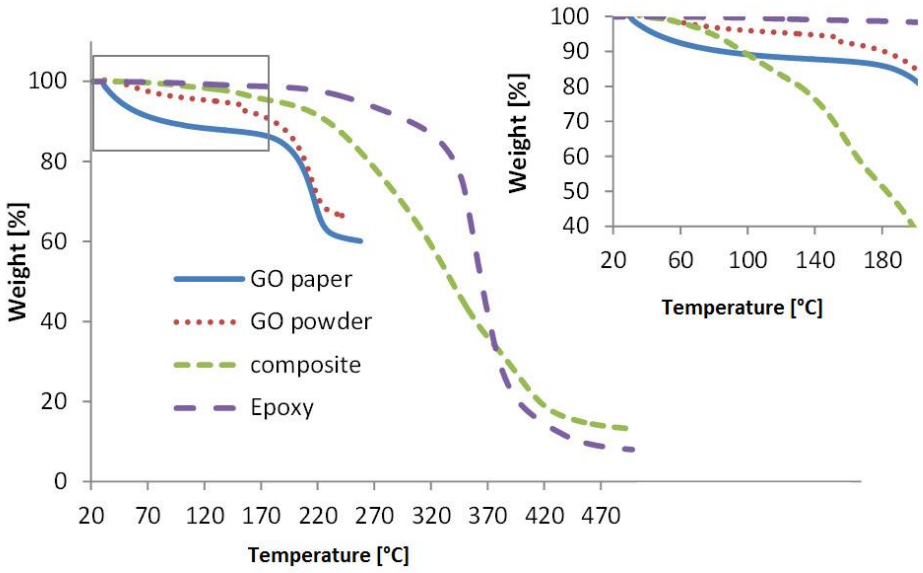

Figure 4-3 TGA results for GO paper, powder, composite and neat epoxy under dynamic heating with ramp rate of 5°C/min. Inset: Normalised weight curve for 10% GO content.

The isothermal case shows that GO decomposition results in a weight loss of 30% which is the same as in the dynamic experiment. This means that the oxygen groups, even the stable ones, such as carbonyl groups in ketone, can be eliminated at 200°C. Therefore, the reduction is sufficient at 200°C. The two small steps in the first 5 minutes point out the evaporation of water and the decomposition of unstable carboxyl at low temperature (inset in Figure 4-4). The real process of isothermal decomposition of GO starts after the first minutes and lasts only 20 minutes. After this period, no further mass loss is observed. In the GO/epoxy composite there is an insignificant mass loss of 10% up to 80°C. This can be explained by the migration of the groups of the base planar of GO to the edges, which proves the reduction but no significant mass loss. Up to 200°C the loss is 50% which indicates that reduction kinetics in the composite material is faster than in dry GO. This could be attributed to the cross linking between the oxygen groups and the hardener.

The weight loss of GO paper is slightly greater than at the beginning of heating compared to the GO powder. This may happen because of the presence of more oxygen due to a different procedure of synthesis of GO as the powder and paper material were from different supplied and the oxygen content can vary significantly depending on the preparation method and its parameters [116; 117].

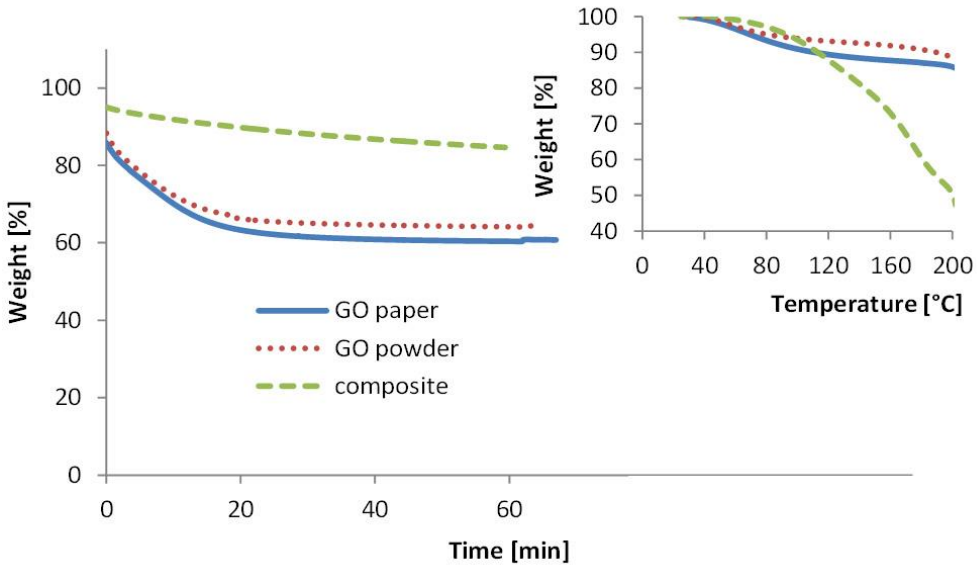

Figure 4-4 TGA results for GO paper, powder and composite under isothermal heating at 200°C. Detail: Normalised weight curve for 10% GO content for the heating until the dwell temperature 200°C with ramp rate of 20°C/min.

4.2.3 Calorimetric evolution of GO reduction

The curves of total enthalpy per unit mass as well as the rate of enthalpy change against temperature are illustrated in Figures from 4-5 to 4-10. As expected, dynamic tests (Figures from 4-5 to 4-10) show that the exothermic peaks of greater rates can be found at higher temperatures. This means that, at low rates, reduction starts and ends earlier. The dry GO paper has similar behaviour to the GO powder which means that GO particles follow the same profile of reduction qualitatively, regardless of the supplier and the production method. A wide exothermic peak is observed at around 215°C for the maximum rate of 5°C/min, whilst at the rate of 1°C/min the peak is found at 200°C.

The evolution of calorimetric effect is different in the composite material (Figures 4-9, 4-10) than in dry particles (Figures from 4-5 to 4-8). It is observed that the reactions occur earlier than in the dry GO confirming that the overall reactivity is higher in the composite. In all materials there are at least two mechanisms in the kinetics. This is explained by the difference in the evolution of the enthalpy change curve in Figures 4-5 and 4-7. The reaction starts at

140°C where the bonds of unstable groups such as carbonyls begin to break gradually. The first mechanism lasts up to 180°C, when the second step progresses faster. This mechanism is not found at the same areas for all temperature rates. The second step of the rate of 1°C/min finishes at a lower temperature (220°C) than at higher rate (Table 4-1). The two different mechanisms are better resolved in the composite case (Figure 4-9). Two processes are observed, with the low rate finishing earlier than the high rate, at 170°C and the peak of the reduction at 147°C. The reaction at the high rate peaks at 157°C with a total enthalpy of 1300 J/g. The first process happens at the same temperature range for the two rates. It starts at 70°C and finishes at 110°C. This can be explained by the fact that the presence of amines may contribute to the reaction by creating bonds with the oxygen groups. Moreover, the particles inside the polymer have undergone dispersion which means the van der Waals interactions have been weakened, and can be more easily broken at lower temperatures. The overall enthalpy of the reaction is unaffected by the rate. However, there is some post cure artefact that is manifested in low rate results of the composite showing higher total enthalpy and longer duration of reaction than at the rate of 1°C /min. The heat flow is lower than for the paper and the powder as it is not normalised to the weight of GO but to the whole weight of the composite. In reality the heat flow is ten times higher than it appears in the graph.

Table 4-1 Temperature range of reduction and overall enthalpy for different rates and materials. The enthalpy in the case of the composite is normalised with respect to the GO content.

Rate [°C/min]	End of reduction [°C]	Temperature range [°C]	Overall enthalpy [J/g]
GO powder			
5	240	100	1239
1	220	80	1242
GO paper			
5	237	97	1285
1	210	70	1289
Composite			
5	210	100	1670
1	170	70	1600

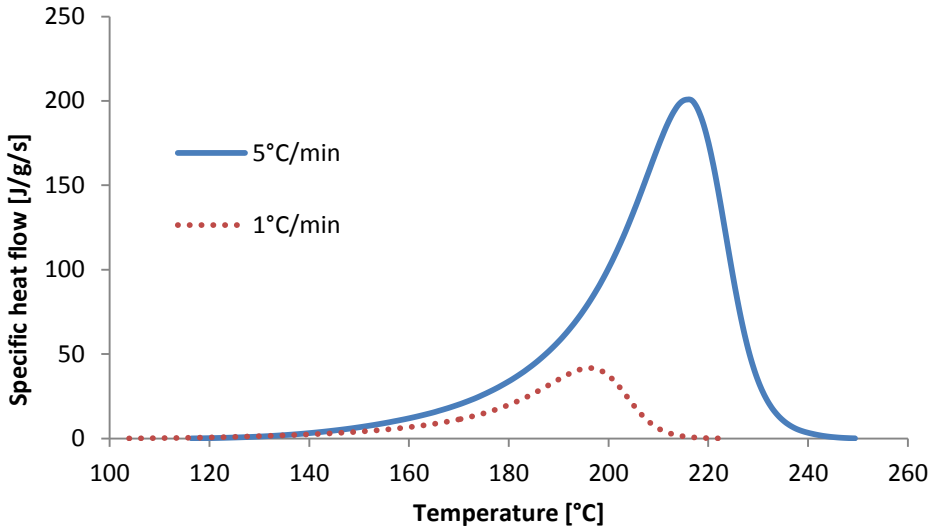

Figure 4-5 Specific heat flow versus temperature of GO powder during dynamic heating up to 260°C.

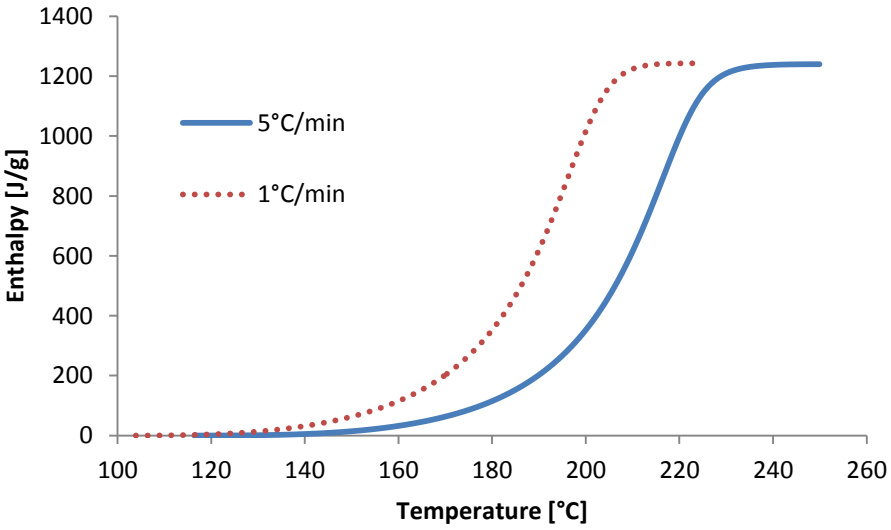

Figure 4-6 Total enthalpy of GO powder during dynamic heating at different rates up to 260°C.

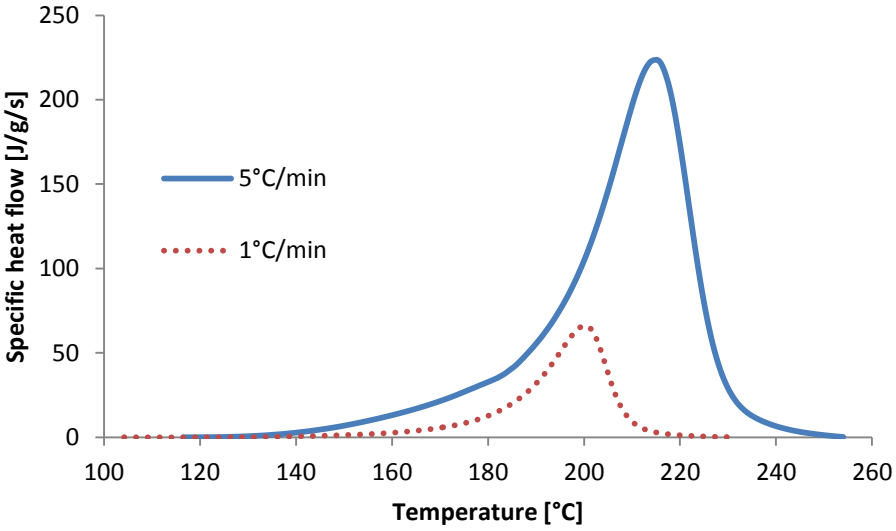

Figure 4-7 Specific heat flow over time of GO paper during dynamic heating up to 260°C.

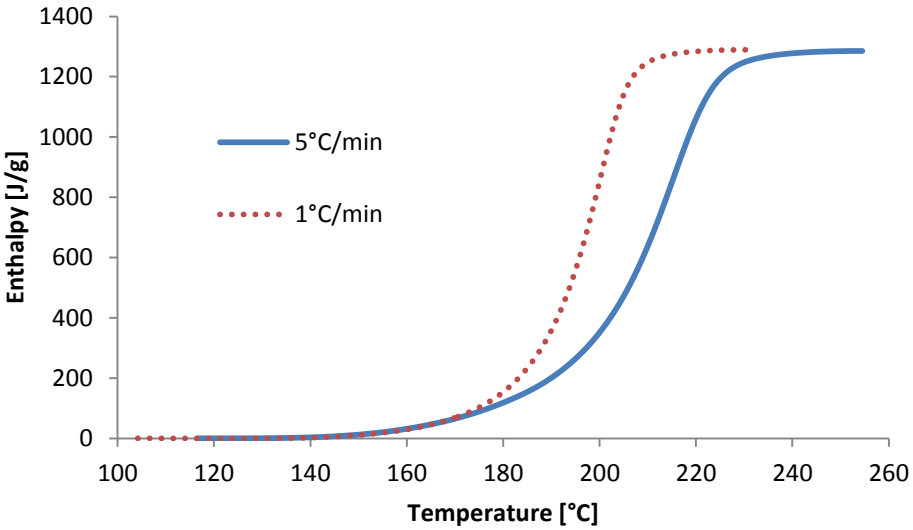

Figure 4-8 Total enthalpy of GO paper during dynamic heating at different rates up to 260°C.

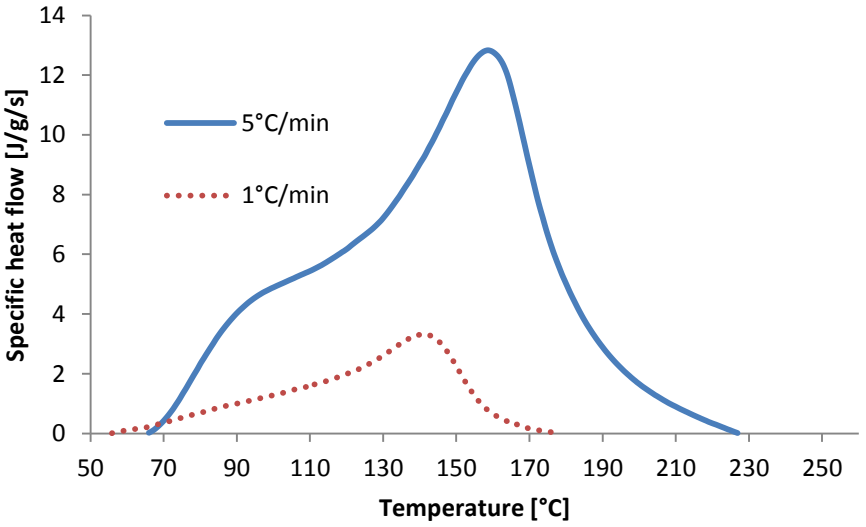

Figure 4-9 Specific heat flow over time of the composite during dynamic heating up to 260°C.

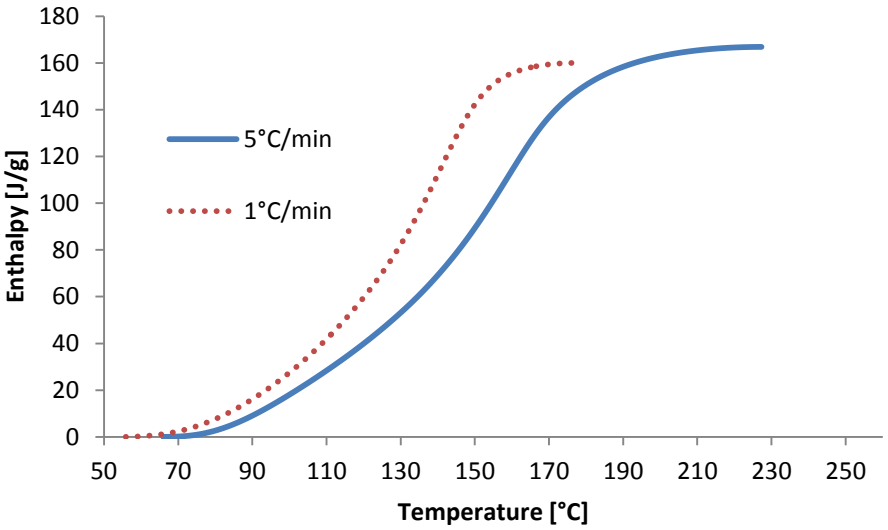

Figure 4-10 Total enthalpy of composite during dynamic heating at different rates up to 260°C.

The results of the isothermal tests at several temperatures are presented in Figures from 4-11 to 4-14. The total enthalpy and the rate of enthalpy change are illustrated against time. Zero time is the time that the material reaches the dwell temperature.

It is observed that the total enthalpy is high at temperatures of 200°C, 220°C and the reaction appears to finish before 10 minutes at 220°C and within 20 minutes at 200°C (Figures 4-11, 4-12). More time is necessary for the completion of reaction at lower temperatures. Different final level of reduction occurs at different temperatures as indicated by the values of total enthalpy. At 220°C and 200°C the enthalpy is 1200 J/g and 1150 J/g respectively. At lower temperatures the enthalpy is reduced to 800 J/g at 180°C and 200 J/g at 160°C.

The results of dynamic tests for the paper and the powder showed that the reaction starts at low temperatures and particularly for the dry particles ends at 220°C at the rate of 5°C/min. This means that in this case of isothermal profile the reaction has already started during heating before the material reaches 220°C. From dynamic results it is known that as the rate of heating increases, the reaction delays, so it can be concluded that the reduction is partly completed when the temperature is 220°C or even 200°C. The integration of the

isothermal raw data was carried out taking into account the heat emitted during heating up at 20°C/min until the temperature equilibrated at a constant value. The temperature dependence of the reduction is prevalent in the case of the composite material. The initial enthalpy of the composite at the dwell temperature is much greater than the particles (Figures 4-11, 4-13, 4-15). This is because the reduction begins much earlier than in the dry GO releasing energy during heating until the dwell temperature.

These results follow expectations regarding the dependence on the heating rate. The rate in composite curves is higher compared to dry particles implying a faster mechanism. This is attributed to the dispersion in the solvent before the incorporation facilitating a faster reaction and to the potential creation of bonding between the amine groups of epoxy and the oxygen groups of GO.

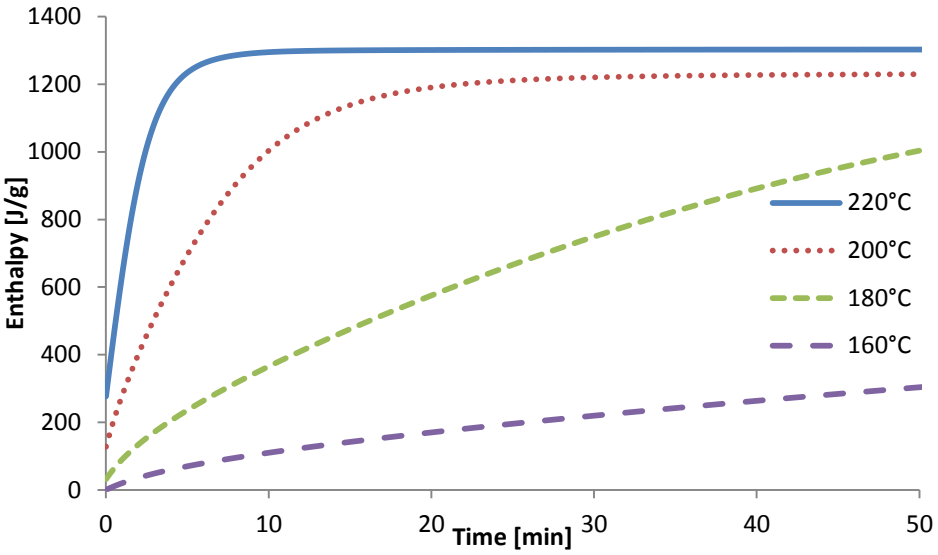

Figure 4-11 Total enthalpy of GO powder during isothermal heating at different temperatures.

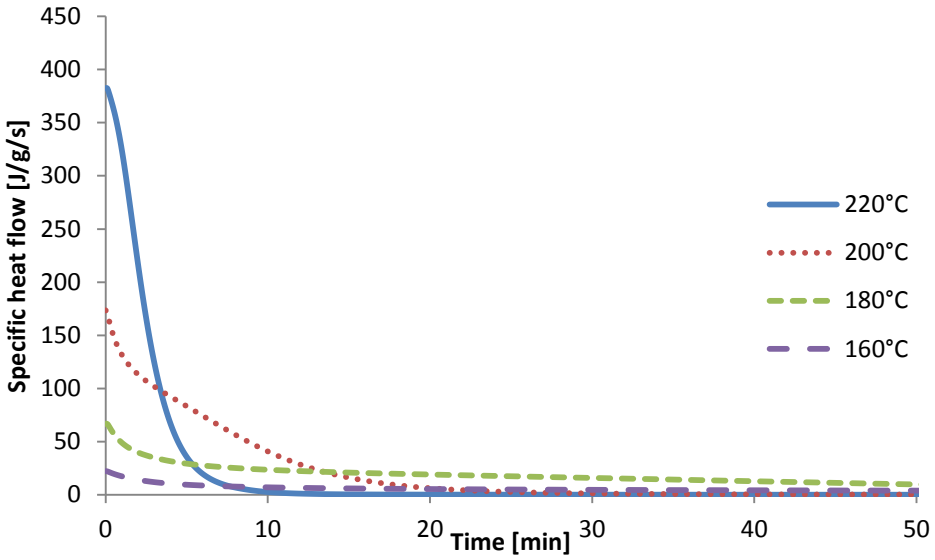

Figure 4-12 Specific heat flow over time of GO powder during isothermal heating at different temperatures.

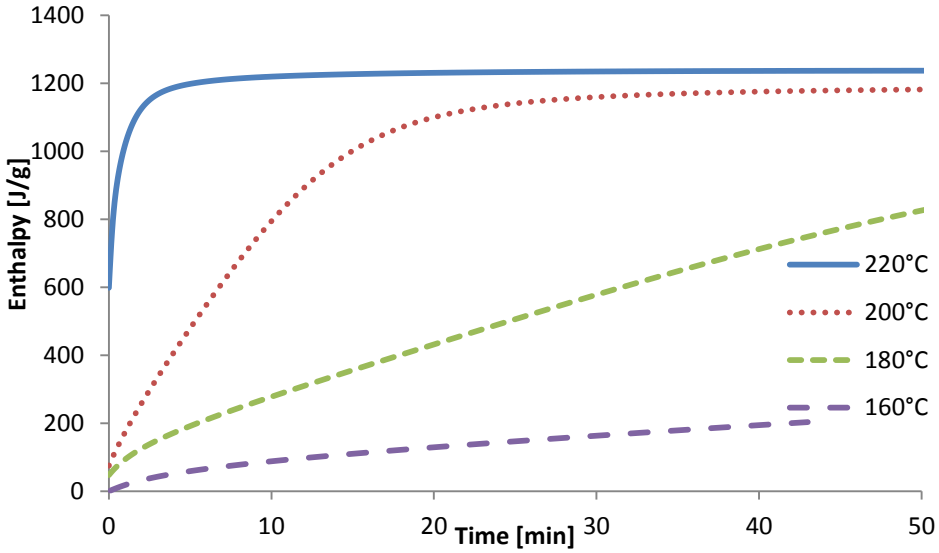

Figure 4-13 Total enthalpy of GO paper during isothermal heating at different temperatures.

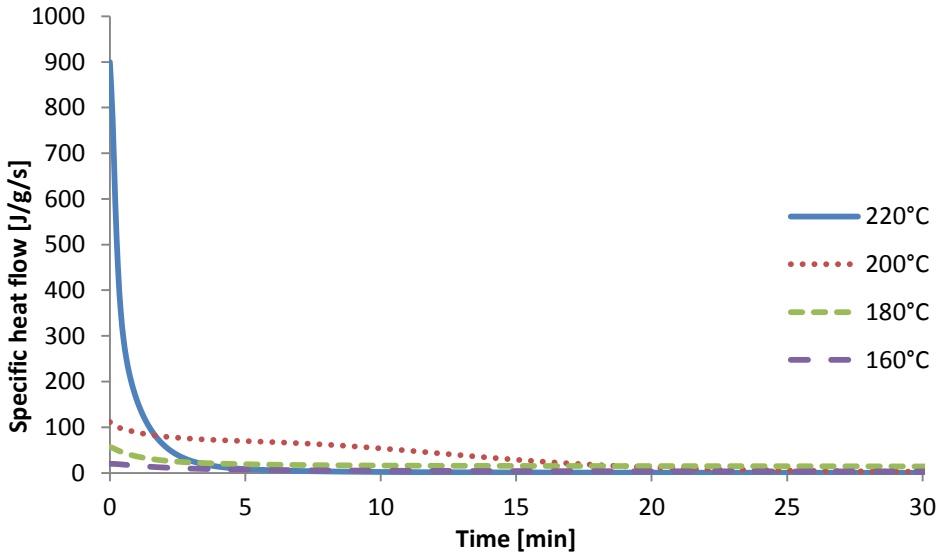

Figure 4-14 Specific heat flow over time of GO paper during isothermal heating at different temperatures.

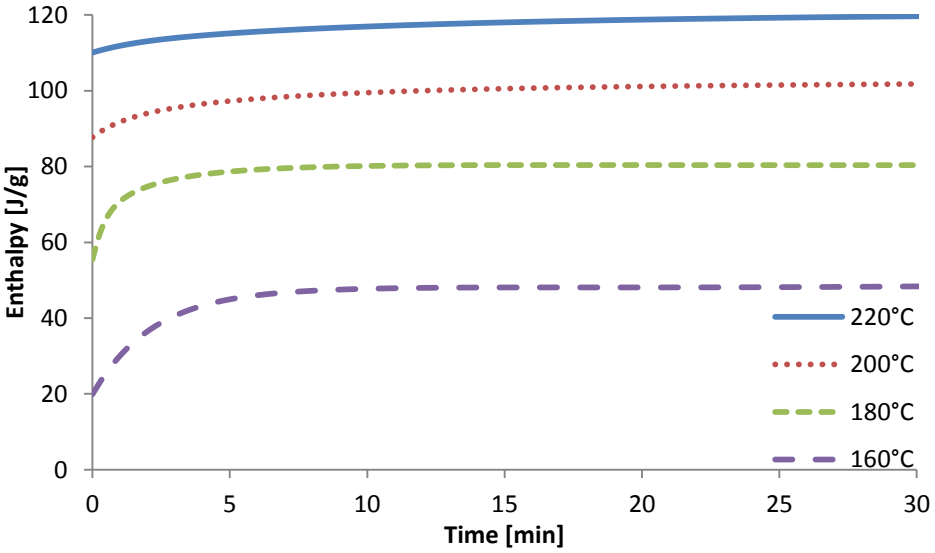

Figure 4-15 Total enthalpy of the composite during isothermal heating at different temperatures.

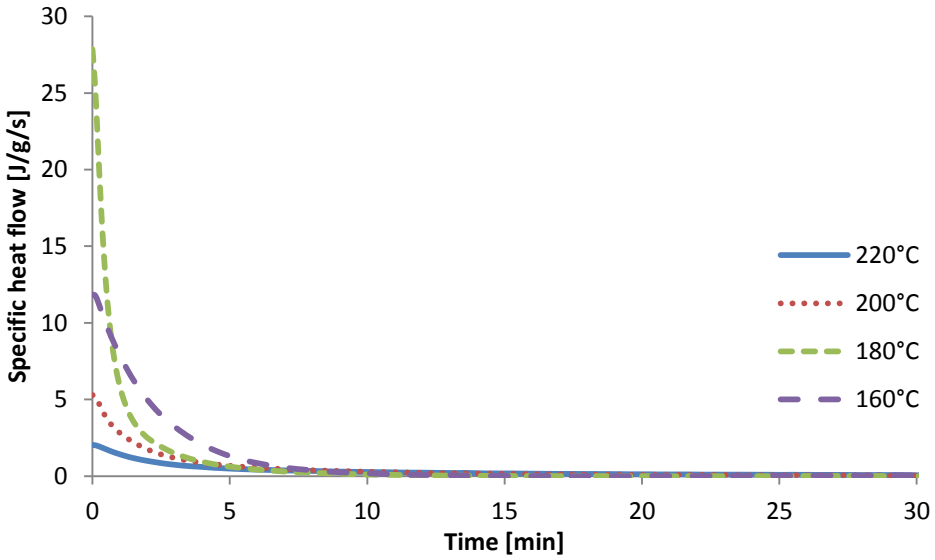

Figure 4-16 Specific heat flow over time of the composite during isothermal heating at different temperatures.

4.2.4 Comparison of mass evolution with calorimetric response

The rate of mass reduction from TGA is compared with the specific heat flux in Figures 4-17 and 4-19. As it can be observed in Figure 4-17 the mass loss starts at about 150°C and its rate is maximised at around 217°C. The heat flow evolution follows the mass loss curve very closely. The mass loss at 50°C is attributed to material dehydration occurring at low temperatures. The small peak in mass loss rate at 150°C is considered an artefact of the experiment.

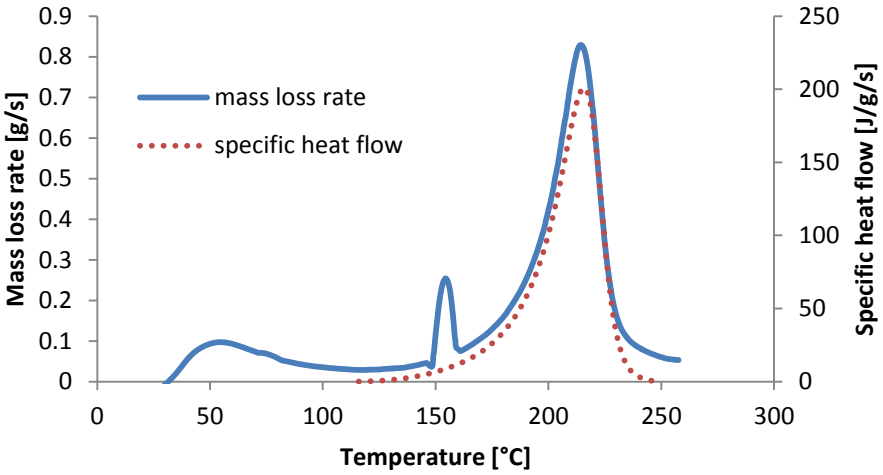

Figure 4-17 TGA and DSC results for GO powder heated dynamically at 5°C/min.

The results in Figure 4-18 for the GO paper show similar evolution of the TGA and the DSC curve. The mass loss rate is low and constant in the temperature range from 100 to 140°C. Starting from 140°C the reduction takes place, showing an increasing mass loss rate up to 217°C. The two steps of reduction are not evident in the TGA curve unlike the specific heat flow. This can be explained by the migration of the planar groups such as carbonyls to the edges. This migration can cause a light increase in exothermic output but the mass flow is constant in the structure. Above 160°C the GO paper begins losing mass in the same way as it emits heat.

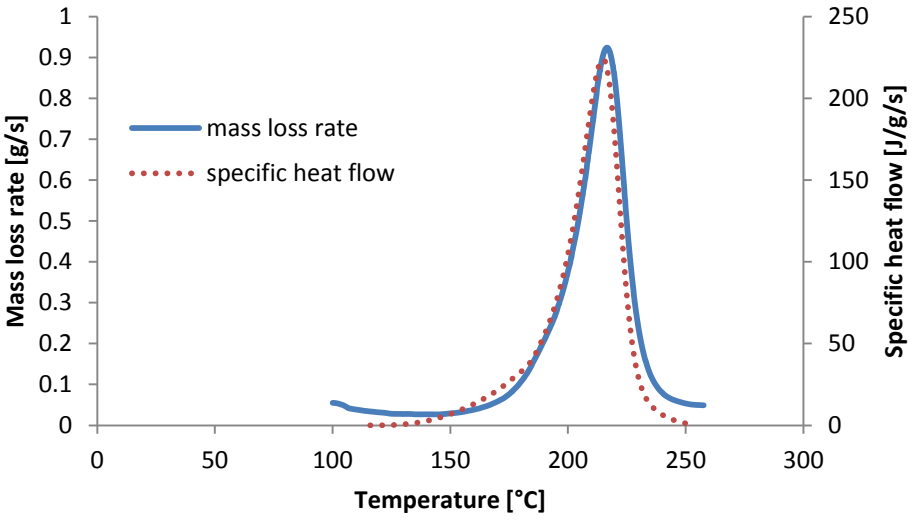

Figure 4-18 TGA and DSC results for GO paper heated dynamically at 5°C/min.

In the composite (Figure 4-19), it can be observed that the main peak temperatures of DSC and TGA coincide at about 157°C. It is expected tha the neat epoxy resin is inert at the range of temperature of these experiments.The first step of reduction is clear at temperatures between 70°C and 140°C and the first peak is evident at around 100°C in both the TGA and DSC results. The mass loss starts earlier in the composite than in the dry particles. At temperatures higher than 157°C the mass loss rate decreases gradually up to 180°C. As the temperature rises above 200°C the mass loss rate starts increasing again due to the decomposition of the resin. The heat flow curve shows a gradual drop towards a plateau beyond the main peak temperature. The two stages of reduction are manifested clearly in both experiments; in the case of TGA the mass loss due to the reduction is superimposed to loss due to other phenomena such emission of volatiles and resin degradation.

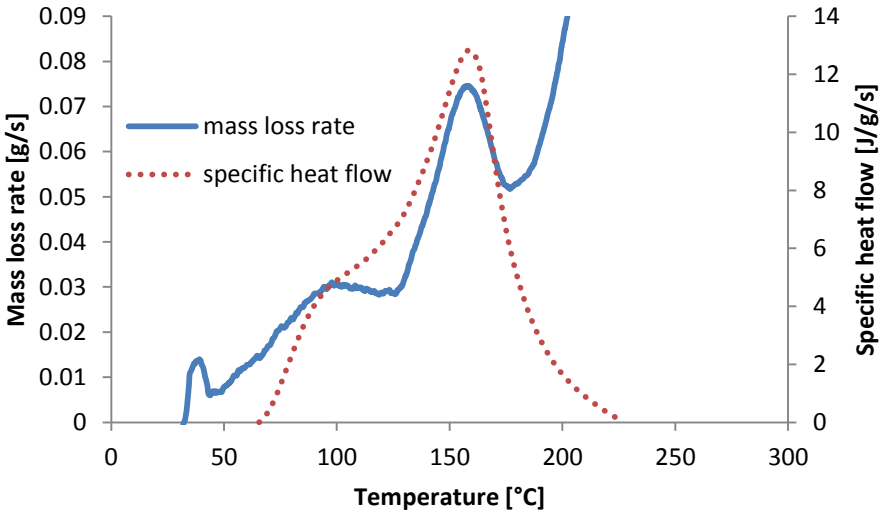

Figure 4-19 TGA and DSC results for the composite, heated dynamically at 5°C/min.

Overall, the TGA and DCS results prove that mass loss and heat flow follow the reduction closely. The mass loss rate progresses in the same way as the heat flow, with maximum values occurring at the same temperature for GO powder, GO paper and the composite.

4.3 Reduction kinetics modelling

The results of calorimetric experiments were utilised to develop a model of reduction kinetics based on an assumption of proportionality between the rate of reaction and the heat emitted. A degree of reduction $\boldsymbol{\beta}$ is defined to characterise the progress of the reaction; the definition concerns only the reduction within the intermediate temperature range of this investigation, which is practically up to 260°C. The degree of reduction is equal to zero at the beginning of the reaction and one when the reduction is considered complete. The model expresses the reaction rate as a function of the degree of reduction and temperature as follows:

$$\frac{d\boldsymbol{\beta}}{dt} = \boldsymbol{f}(\boldsymbol{\beta}, \boldsymbol{T}) \tag{4}$$

where T is the temperature and t the time.

The model selected uses two n-th order terms to represent the two processes identified in dynamic DSC experiments [122]. This is expressed as follows:

$$\frac{d\beta}{dt} = A_1 e^{-E_1/RT}(1-\beta)^m + A_2 e^{-E_2/RT}(1-\beta)^n \quad (5)$$

Here A_1, A_2, E_1, E_2, m and n are the pre-exponential factors, activation energies and exponents of the first and second mechanism respectively and R is the universal gas constant. The parameters of the model were estimated using the experimental data and non-linear least square fitting and are reported in Table 4-2. The calculations were carried out selecting initial values using the Generalized Reduced Gradient Algorithm implemented in Microsoft Excel.

Table 4-2 Reduction kinetics equation coefficients of GO paper and powder

	GO paper	GO powder
E_1 (J/mole)	143230	144200
E_2 (J/mole)	76180	77190
A_1 (1/s)	1.40×10^{13}	1.50×10^{13}
A_2 (1/s)	2.07×10^{4}	1.77×10^{4}
m	0.94	0.82
n	5.33	5.65
R	8.3144	8.3144

The quality of the fit for the GO paper and the dry powder is illustrated in Figures from 4-20 to 23. It should be noted that an additional experiment at 0.2°C/min was added to the data sets to extend the envelope of validity of the model. It can be observed that the model fits the data closely. This model can be integrated numerically to predict the evolution of the reduction reaction if the thermal profile is known. This means that the process of reduction can be simulated within a heat transfer model representing the application of the process to a component. This would allow prediction of the distribution of the reduction state within the component which could be correlated with a distribution of electrical conductivity. Therefore, the kinetics model could serve as the basis for process desing allowing tailoring of localised variations in electrical conductivity specific to the needs of the application and component.

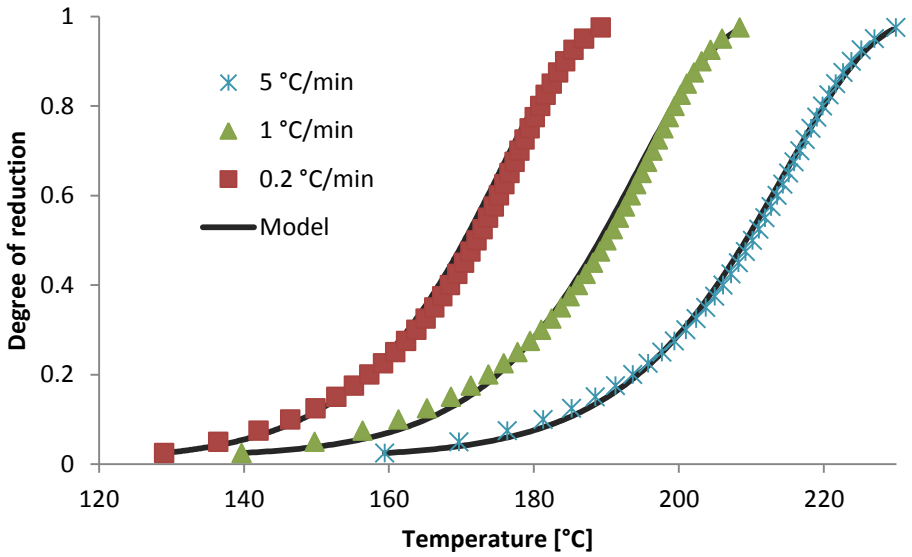

Figure 4-20 Degree of reduction as a function of temperature for GO powder under dynamic heating at different rates.

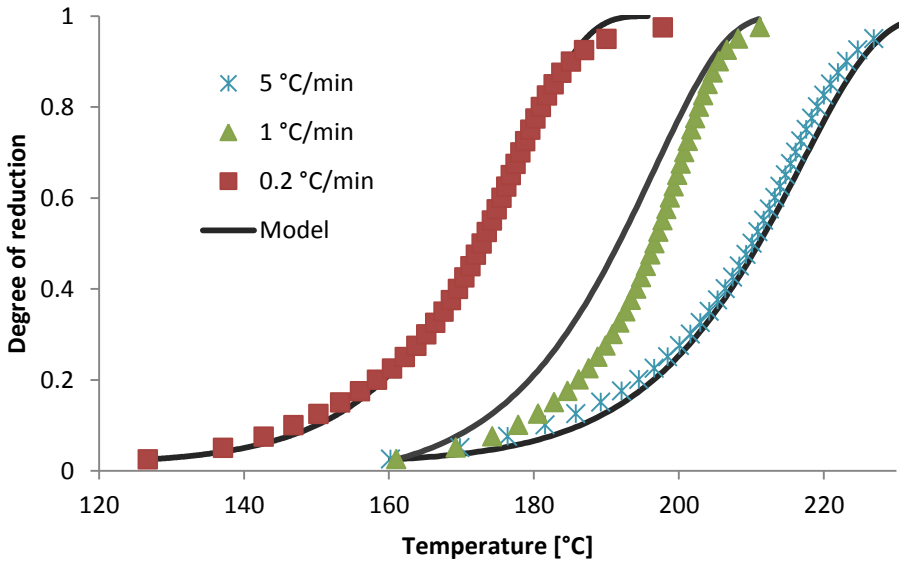

Figure 4-21 Degree of reduction as a function of temperature for GO paper under dynamic heating at different rates.

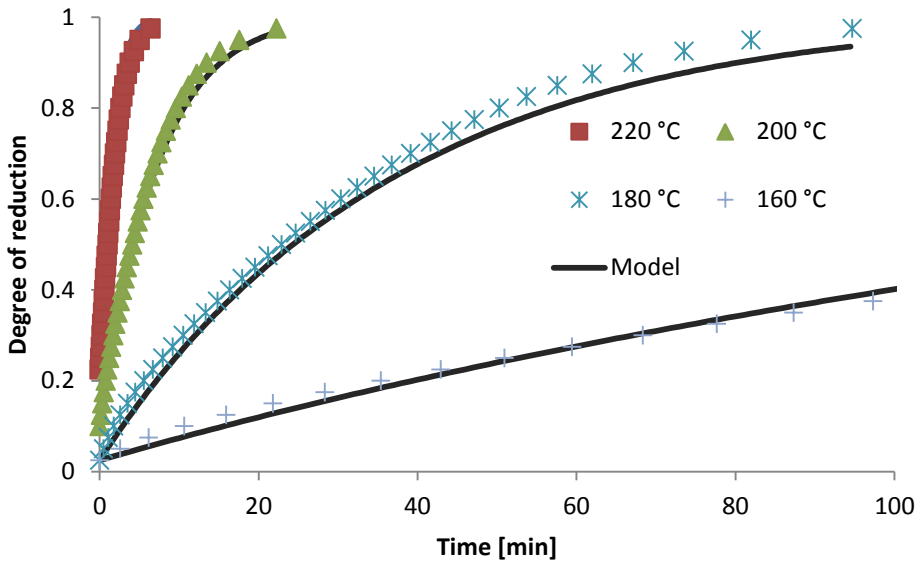

Figure 4-22 Degree of reduction as a function of time for GO powder under isothermal heating at different temperatures.

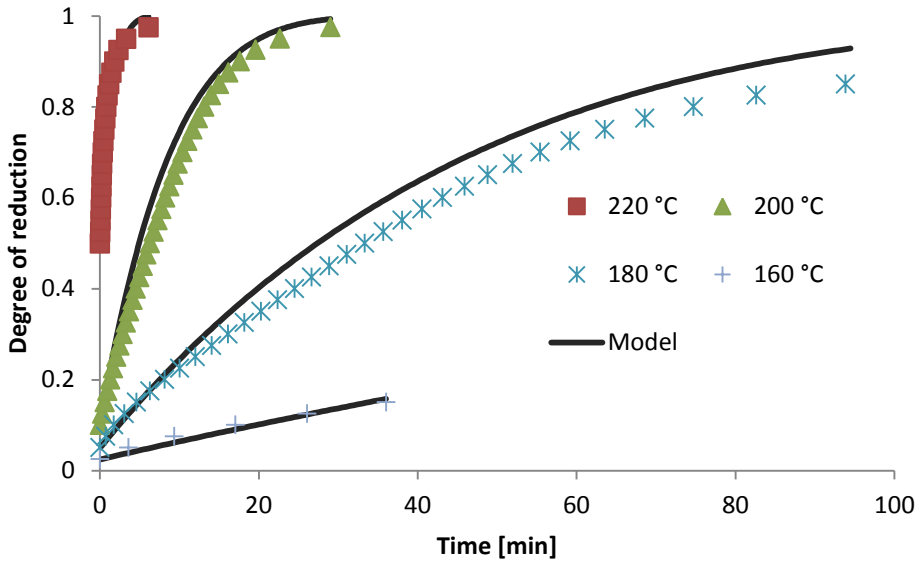

Figure 4-23 Degree of reduction as a function of time for GO powder under isothermal heating at different temperatures.

4.4 Electrical characterisation

The conductivity spectra evolution in dynamic heating conditions for the GO paper and the composite is illustrated in Figures from 4-24 to 4-29. The spectrum of real conductivity of GO paper heated at 5 °C /min at 100°C shows a plateau up to 10 Hz and a linear increase in a log-log scale over this frequency.

This is typical behaviour of a lossy insulator [123]. In agreement with calorimetric and gravimetric results at 100°C the material still contains the oxygen groups preventing electronic transfer. This behaviour is followed up to a temperature below 180°C. The conductivity increases significantly at 220°C and reaches the highest value at the maximum temperature of heating 260°C. The spectrum shifts to higher frequencies as the conductivity of the material increases. The range at which the conductivity increases significantly coincides with the temperature range of fast reduction in DSC and TGA experiments. The conductivity was measured again after cooling down at ambient temperature. It should be noted that there are some regions of decreasing conductivity with frequency in some of the spectra. These are experimental artefacts of two types. At temperatures of fast reduction, e.g. the 180°C spectrum in Figure 4-24, this effect appears at low frequencies due to the small time lag between successive measurements that are considered isochronal. At high temperature, e.g. the spectrum at 260°C in Figure 4-24, this effect appears at high frequencies due to limitation of the measuring setup for highly conductive materials.

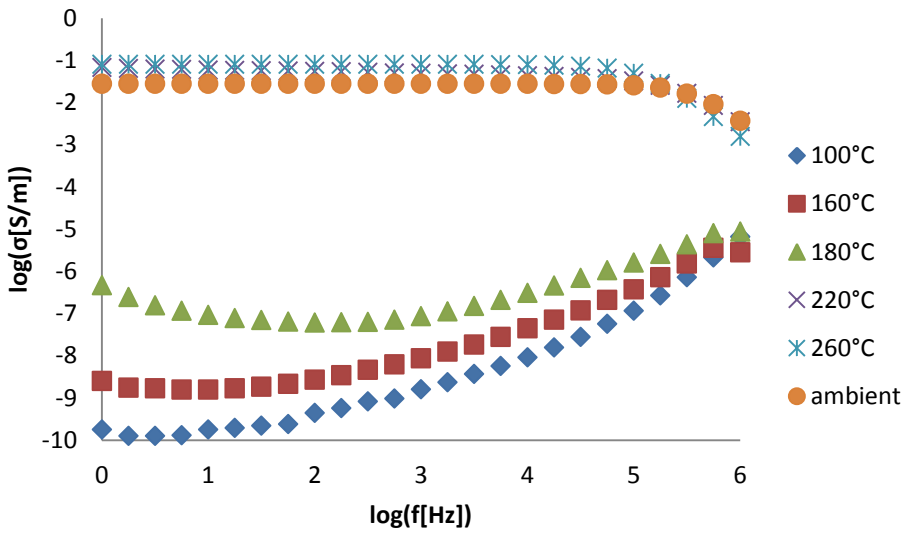

Figure 4-24 Real conductivity spectra for GO paper during dynamic heating at 5°C/min.

At the lower rate of 1°C/min (Figure 4-25) there is enough time to develop conductivity properties at lower temperatures in agreement with the results of calorimetry. The spectrum at 160°C shows a plateau covering a range of frequencies up to 1000 Hz At 180°C the plateau finally covers the overall range of frequencies up to 1 MHz. The material is conductive with a low conductivity of ~10^{-5} S/m. Further heating above 180°C moves the spectra towards higher values of conductivity. The corresponding to 220°C and 260°C are very close to each other with conductivity in the 10^{-1} S/m range.

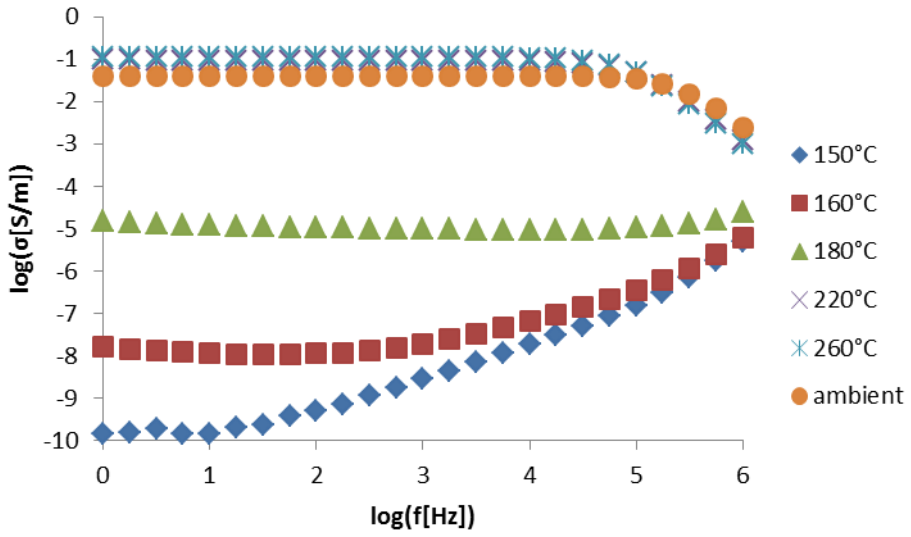

Figure 4-25 Real conductivity spectra for GO paper during dynamic heating at 1°C/min.

In the case of slow heating at 0.2°C/min, (Figure 4-26) the material reaches a fully conductive behaviour at 160°C there is a uniform plateau across all frequencies with a low conductivity of 10^{-5} S/m. The conductivity increases progressively up to 260°C by about four orders of magnitude.

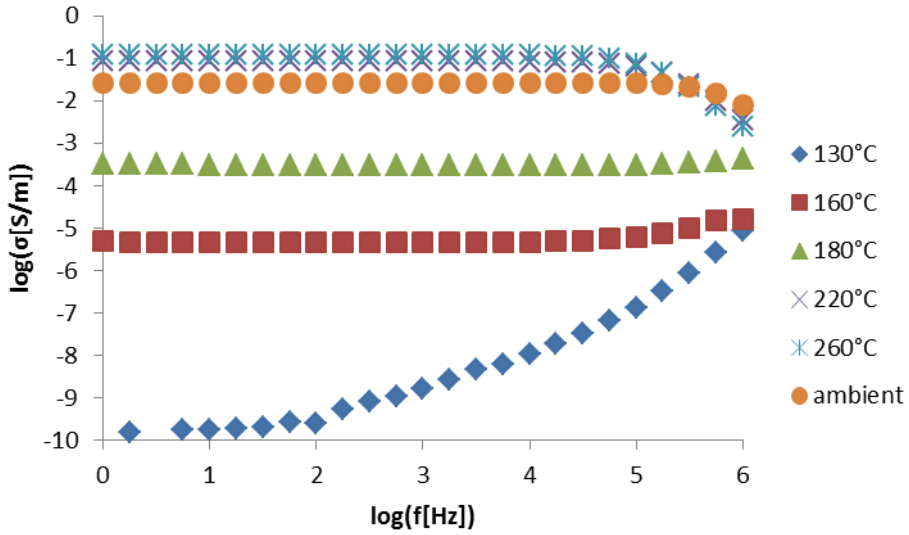

Figure 4-26 Real conductivity spectra for GO paper during dynamic heating at 0.2°C/min.

The evolution of real conductivity spectra under dynamic conditions for the composite material is illustrated in Figures 4-27 and 4-29. Similarly to the GO paper results, the spectra show a wide plateau at lower temperatures when the rate of the thermal profile becomes slower. The spectra progress gradually from the insulating properties to conductivity. The initial spectra show a plateau region and conductivity about three orders of magnitude higher than in the case of GO paper. This is due to the electrical behaviour of the epoxy, which is over its glass transition temperature (25 °C) at the temperature range of the measurements. The final conductivity is slightly lower for the composite than for the GO paper which is a gain attributed to the presence of the polymer.

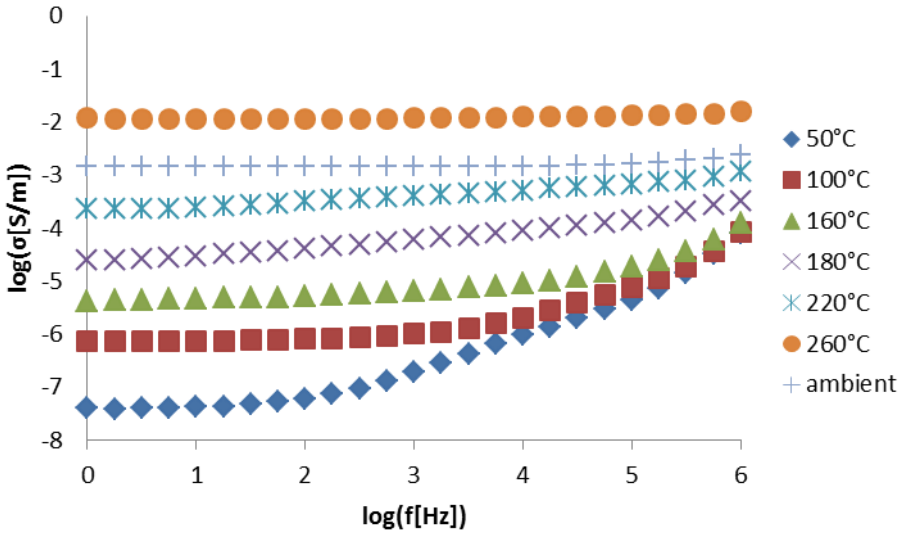

Figure 4-27 Real conductivity spectra for the composite during dynamic heating at 5°C/min.

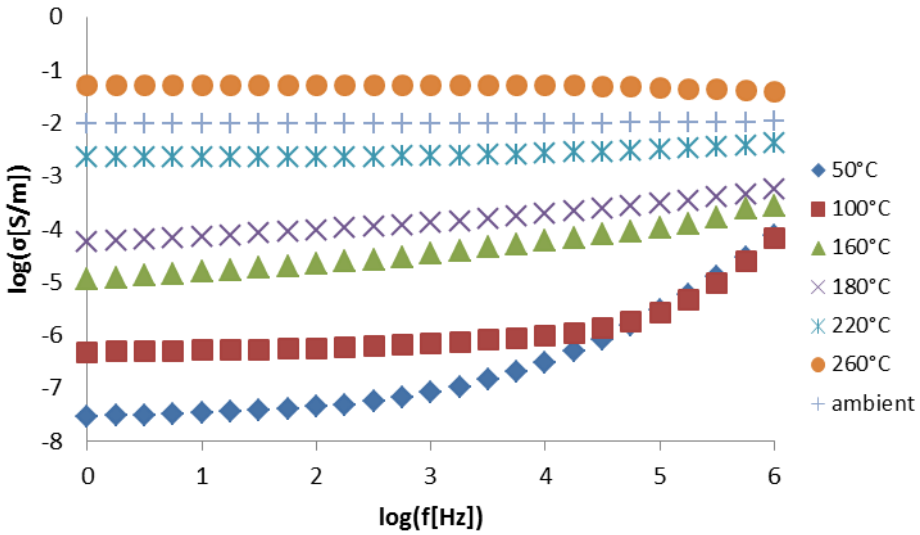

Figure 4-28 Real conductivity spectra for the composite during dynamic heating at 1°C/min.

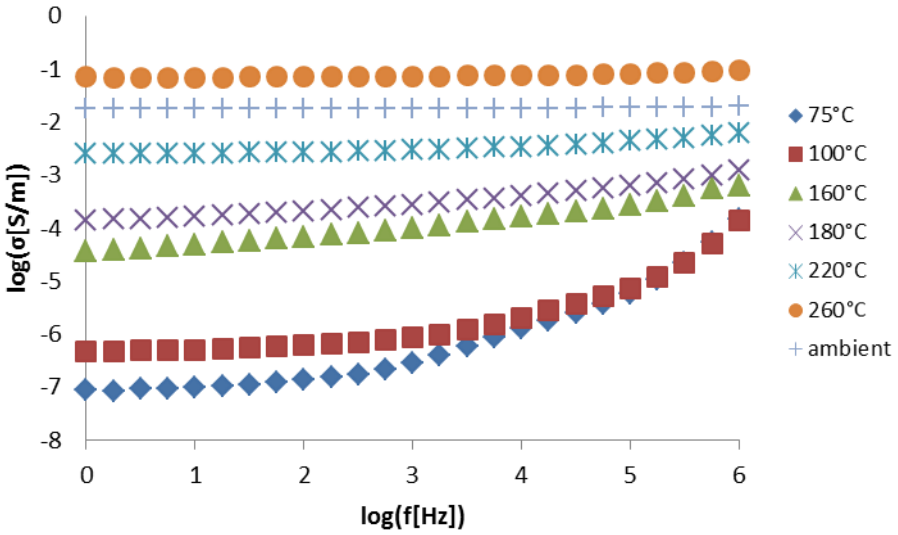

Figure 4-29 Real conductivity spectra for the composite during dynamic heating at 0.2°C/min.

Figures 4-30-37 illustrate the conductivity spectra evolution during isothermal heating at 160°C-220°C for GO paper and the composite. The GO paper is not conductive when it reaches the temperature of 220°C (Figure 4-30) due to the high ramp rate used to reach the dwell temperature and considering that a set of reading takes approximately two minutes. The material becomes conductive within 5 minutes at 220°C and improves to ~10^{-2} S/m after 290 min.

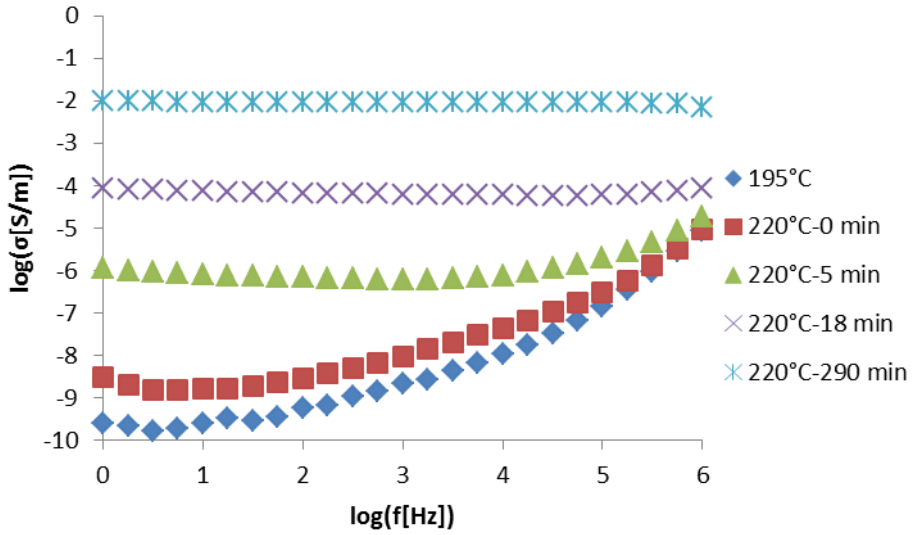

Figure 4-30 Real conductivity spectra for GO paper during isothermal heating at 220°C.

The transition of GO paper from insulator to conductor is fast at 200°C. However, the increase is slower than at 220°C. The GO paper preserves its conductivity cooling down to ambient temperature at the end of the isothermal experiment.

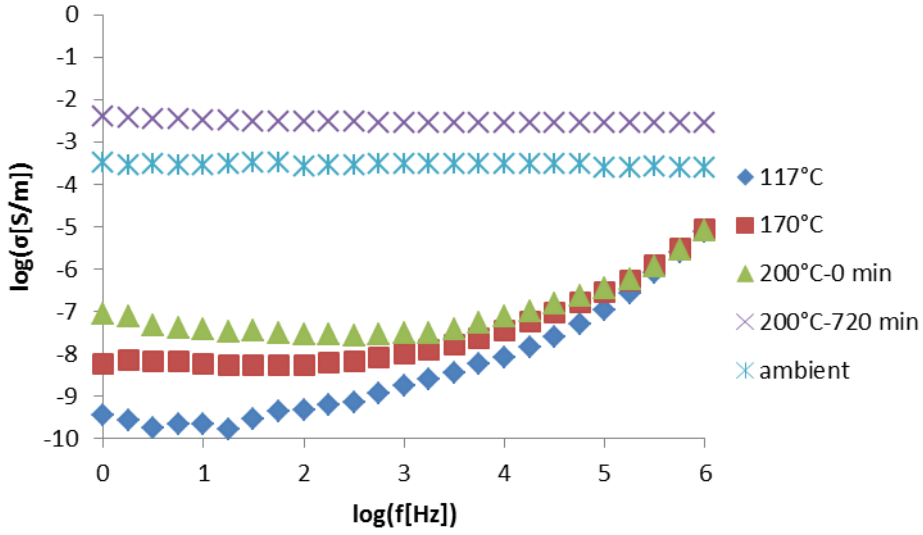

Figure 4-31 Real conductivity spectra for GO paper during isothermal heating at 200°C

The transition during the 180°C experiment (Figure 4-32) is slower than at 200°C and 220°C. After 4 minutes at 180°C the material is still an insulator. After 30 minutes, the conductivity plateau covers a wider range of low frequencies; still at higher frequencies the capacitive behaviour is evident. The GO paper becomes conductive after 140 min with a conductivity of about 2 10^{-5} S/m which increases by more than three orders of magnitude after 900 min and is preserved upon cooling to ambient temperature.

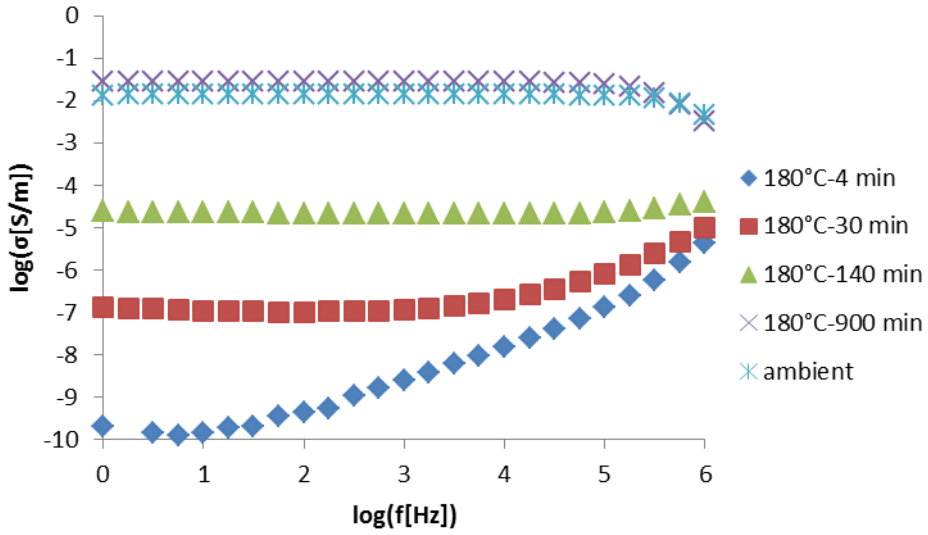

Figure 4-32 Real conductivity spectra for GO paper during isothermal heating at 180°C.

In the 160°C experiment (Figure 4-33) the transition occurs well after 140 min, whilst the conductivity reaches a value 10^{-3} S/m after 1440 minutes. The conductive behaviour is preserved after cooling with a conductivity close to 10^{-4} S/m.

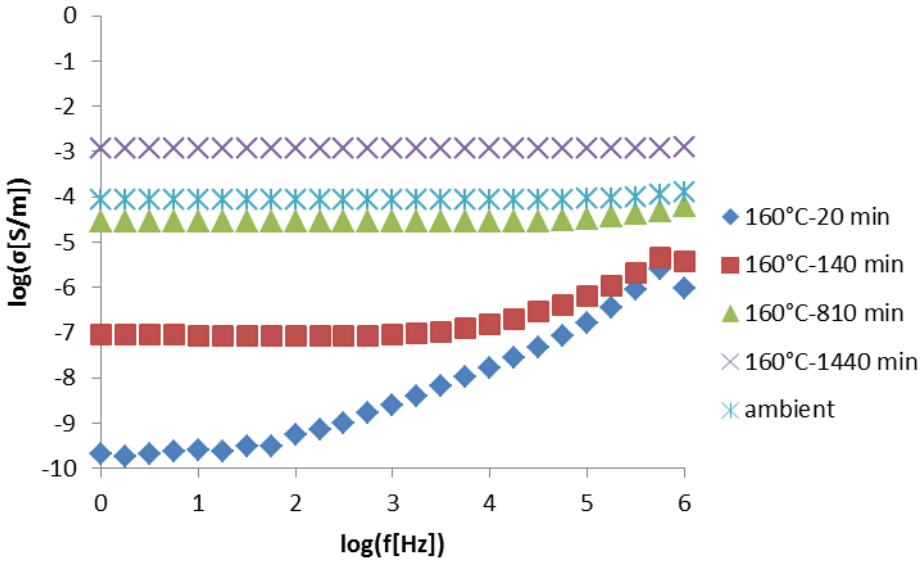

Figure 4-33 Real conductivity spectra for GO paper during isothermal heating at 160°C.

In the case of the composite material conductive behaviour is attained quickly under isothermal conditions (Figures 4-34-37). The spectra show a wide plateau when temperature reaches the dwell temperature. This implies a faster reduction in the composite than in the GO paper, a result which is in agreement with the results of DSC and can be attributed to the effect of having an already dispersed morphology in the composite but also to potential interactions of the oxygen containing groups in GO with the amine of the epoxy matrix. At 160°C (Figure 4-37) the conductivity is significantly lower and the plateau not uniform. This is due to the partial reduction of GO particles in the composite, which has a significant influence in the conductive behaviour of the material governed by particle percolation. It should be noted that the conductivity of the neat epoxy increases slightly at high temperatures but it returns to its insulating behaviour after cooling down.

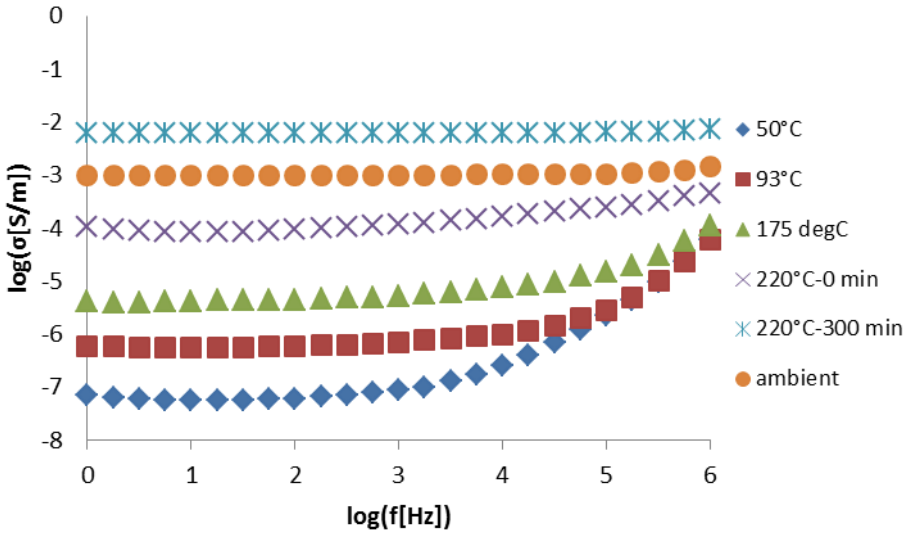

Figure 4-34 Real conductivity spectra for the composite during isothermal heating at 220°C.

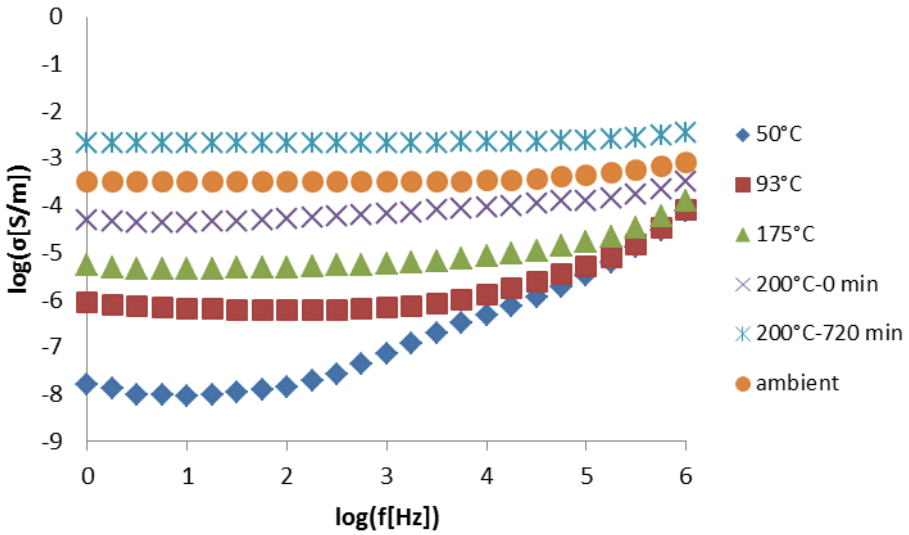

Figure 4-35 Real conductivity spectra for the composite during isothermal heating at 200°C.

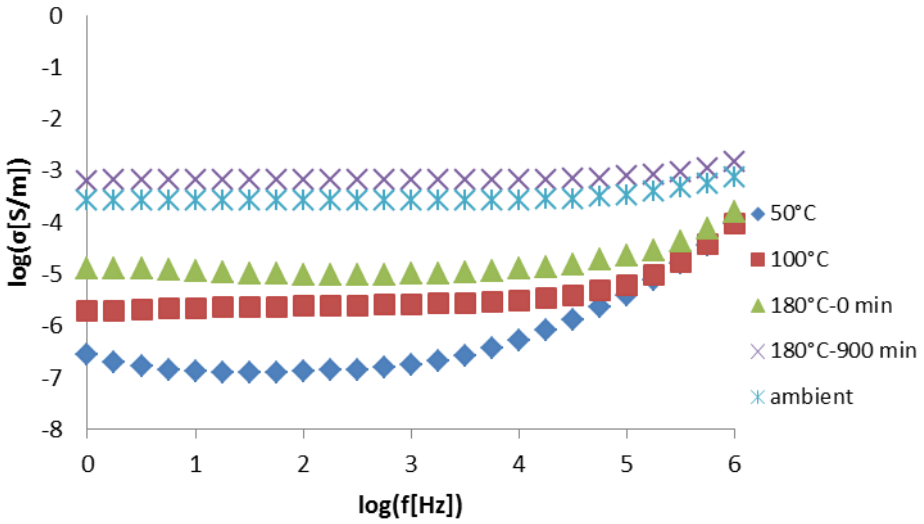

Figure 4-36 Real conductivity spectra for the composite during isothermal heating at 180°C

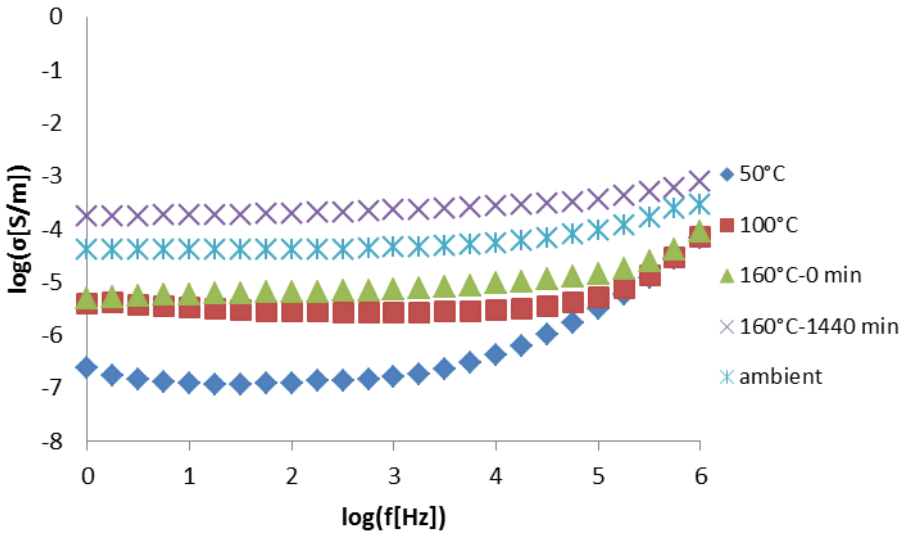

Figure 4-37 Real conductivity spectra for the composite during isothermal heating at 160°C.

The final conductivity at ambient temperature after reduction in presented in Figure 4-38. The GO paper has the greatest conductivity especially after dynamic heating. In this case the conductivity at ambient temperature does depend on the rate of heating. In contrast, in the case of isothermal experiments the GO paper conductivity depends on temperature.

In the case of the composite there is a clear dependence on the temperature and the temperature rate. The conductivity after dynamic heating of 5°C/min rate is 0.0014 S/m. As the rate decreases the conductivity at ambient temperature is higher. At a rate of 1°C/min the conductivity is 0.01 S/m, while it reaches ~0.02 S/m at 0.2°C/min. Isothermal reduction is adequate for increasing conductivity but not as efficient as dynamic heating. Reduction at 160°C results in low conductivity at ambient temperature ($4x10^{-5}$ S/m). Conductivity rises gradually with increasing temperature. It reaches $2.6x10^{-4}$ S/m after the 180°C experiment, whilst there is a further increase to $3.2x10^{-4}$ S/m after reduction at 200°C. In the case of reduction at 220°C the final conductivity reaches a value close to10^{-3} S/m.

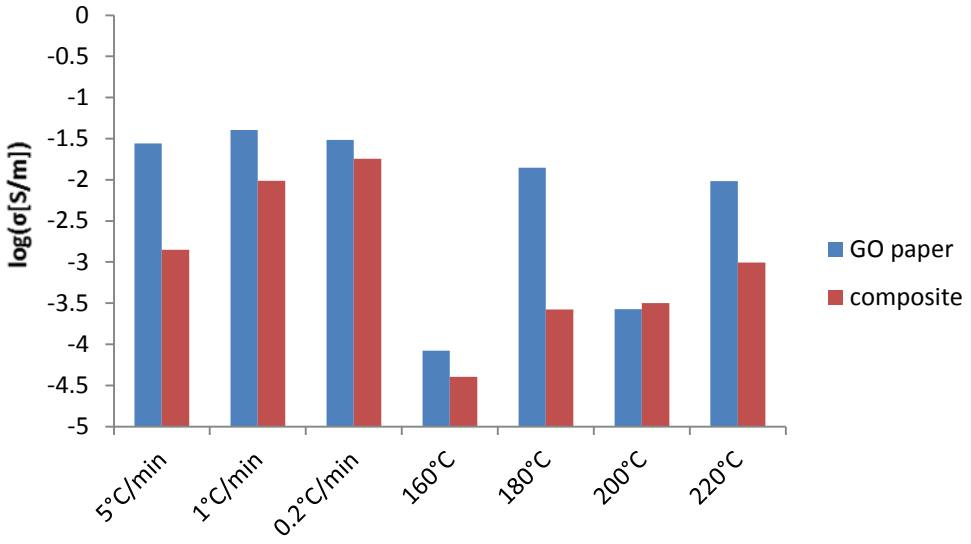

Figure 4-38 GO paper and composite conductivity after the end of reduction at ambient temperature.

These observations are confirmed when the DC conductivity evolution is examined (Figures 4-39-42). The DC conductivity is the average of AC conductivities at low frequencies. Figure 4-39 shows the conductivity evolution of GO paper at the three different heating rates. At low rates of 1°C/min and 0.2°C/min two steps appear in the curve which confirm the existence of two mechanisms in the reduction process.

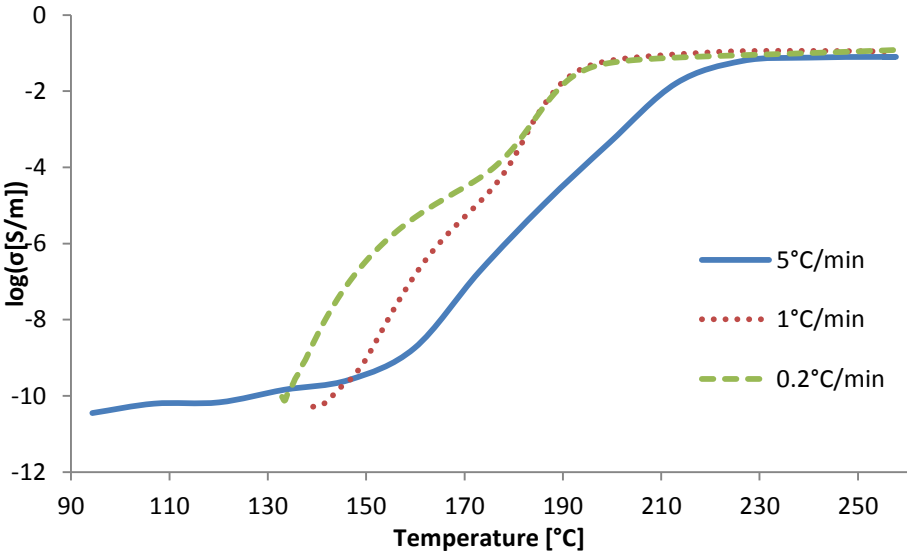

Figure 4-39 DC conductivity of GO paper during dynamic heating at 5, 1 and 0.2°C/min.

The DC conductivity evolution for GO paper under isothermal conditions is presented in Figure 4-40. The conductivity increases gradually at 160°C and does not reach a plateau value within the time range shown in Figure 4-40. As the temperature increases the conductivity increase accelerates

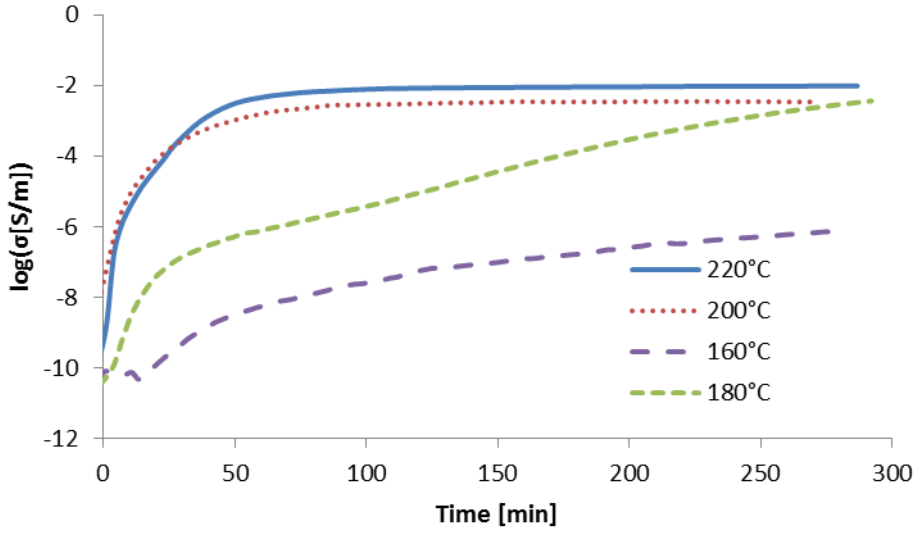

Figure 4-40 DC conductivity of GO paper during isothermal heating at 220, 200, 180 and160°C.

The evolution of conductivity for the composite is presented in Figures 4-41 and 4-42. Similarly to GO paper the conductivity spectra are shifted to higher temperatures as the heating rate increases. However, the sensitivity to temperature appears to be stronger in the composite with the curves at different rates appearing closer than in the case of GO paper. In addition, the composite conductivity reaches a plateau faster than in the paper in isothermal tests (Figure 4-42). The conductivity plateau value increases with increasing temperature, with a sensitivity that is significantly greater than in the case of the GO paper. This happens because the incorporation in the composite accelerates the reduction process.

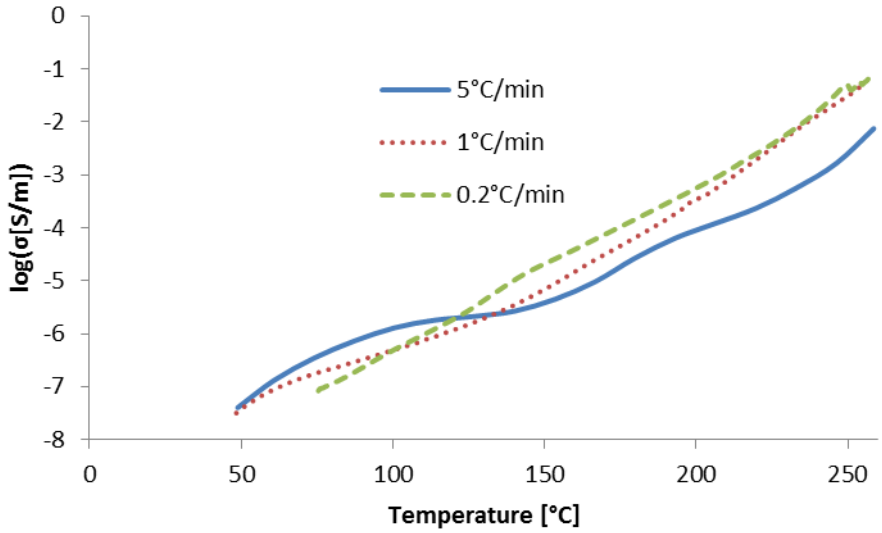

Figure 4-41 DC conductivity of the composite during dynamic heating at 5, 1 and 0.2°C/min.

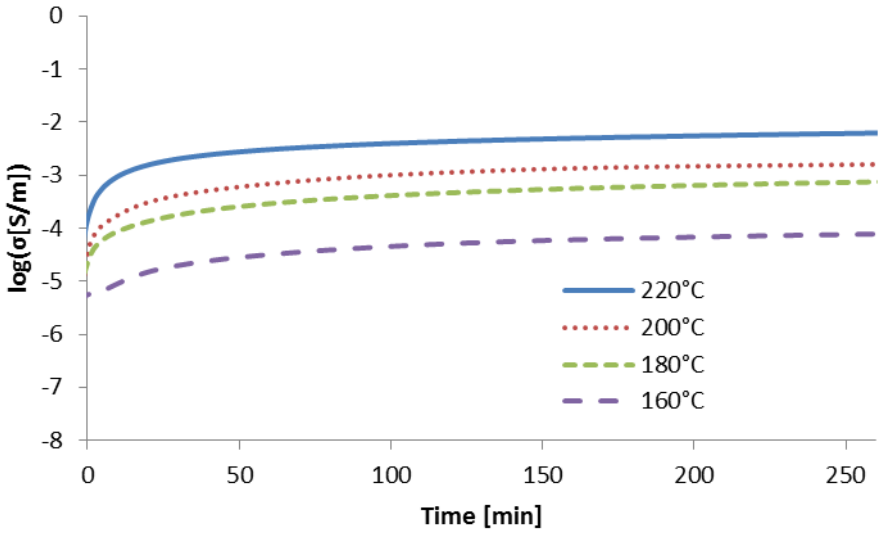

Figure 4-42 DC conductivity of the composite during isothermal heating at 220, 200, 180 and160°C.

4.5 Investigation of laser radiation induced reduction

Stereoscopic images in Figure 4–43 show the pattern generated on the composite surface by pulsed laser. This corresponds to condition 8 (Table 3–2) where a beam of 5 mm diameter was used with average power of 1.53 W applied for 2 ms. The silver coloured regions indicate the areas of rGO in epoxy. The irradiation focused on these areas was converted into local heat and resulted in the reduction of the material. The same colour achieved in the case of the continuous laser where it is observed that the heat spread continuously along the length of the sample (Figure 4–44). Although the average power in this case is 0.982 W which is lower than in the case of Figure 4–43, the surface appears more affected. This is attributed to both the smaller beam diameter focused on the specific area and the duration of irradiation

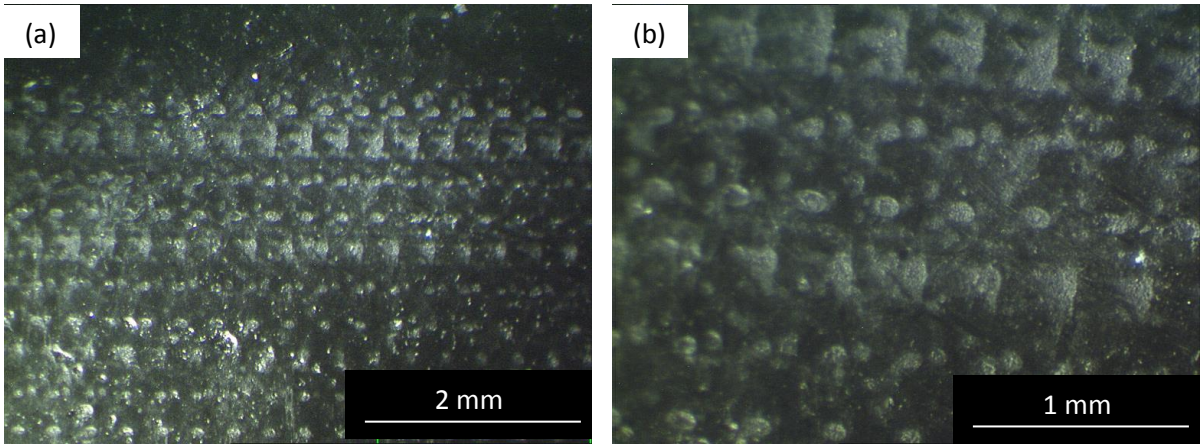

Figure 4-43 Treated surface by pulsed laser with beam size of 5 mm and average power of 1.53 W (condition 8).

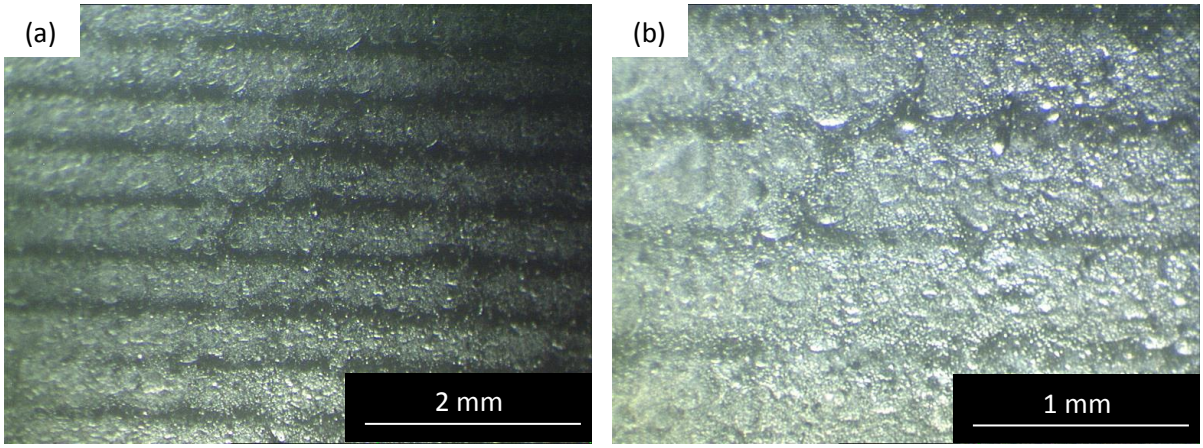

Figure 4-44 Treated surface by continuous laser with beam size of 0.8 mm and average power of 0.982 W (condition 20).

Figure 4–45 summarises the results of conductivity for each case in Table 3-2. In the case of pulse laser the material was degraded when the frequency and the pulse duration were high or the beam size was small (conditions 1, 2, 11). Although the conductivity is high (condition 1, 2, 11) the composite was damaged. On the other hand, changing the beam size to a bigger diameter (from 5 mm to 10 mm), the energy is distributed in a larger area on the material. Combination of a large beam size and low frequency of 10 Hz yields unsatisfactory conductivity. Finding a correct combination of parameters in order to reach a balance for a conductive and non-degraded composite is critical. A large beam size and high frequency (condition 5: beam size 10 mm,

20 Hz frequency, and condition 6 with beam size 10 mm and 15 Hz frequency) is a sufficient combination to obtain satisfactory conductivity without degradation. Similarly, a smaller beam size and lower frequency (condition 10: beam size 6 mm and 10 Hz frequency) can achieve a satisfactory outcome.

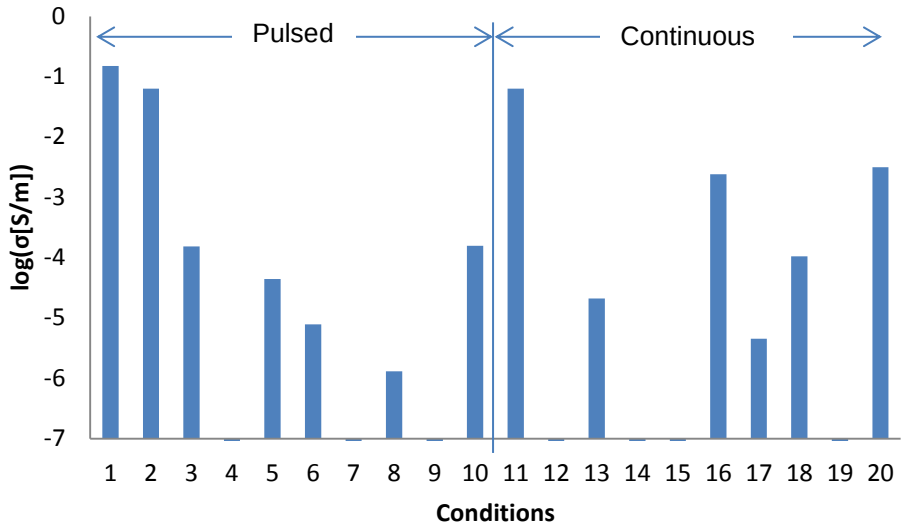

Figure 4-45 Summary of conductivity results for all cases of pulsed and continuous laser on epoxy with 10 wt% GO. Each case is presented in detail in Table 3–2.

The parameters of continuous laser that could be controlled were the beam size, the track distance and the average power. A beam diameter of 0.8 mm is too low and has great influence on the laser energy concentration on a local area. The conductivity is not only affected by the average power, but also by the beam size which irradiated the target surface. However, excessive power results in resin degradation. Electrical properties are much easier to be manipulated with continuous laser. Selecting a beam diameter of 4 mm and average power of 2.995 W yields satisfactory conductivity for a track distance of 2 mm (condition 17). For a lower track distance the beam tends to generate overlap and the conductivity is greater (conditions 16, 18).

4.6 Development of a method for the conductivity grading of graphene oxide based composites

The design of the experimental setup used for producing a conductivity grading is illustrated in Figure 4–46. The aim of this development is to demonstrate how the concept can be implemented physically. The composite material was cured inside a glass tube following the recommended cure cycle. A part of the composite cured rod was fitted in a cylindrical copper tube surrounded by a heating element. The embedded length was 25 mm and the other part of the rod protruded from the cylinder. A monitoring thermocouple was placed in a hole on the copper heating element. Three thermocouples were immersed in the composite rod at three different points through the length in order to take records of the actual temperature (Figure 4–46b). The programmed temperature was set at 220°C. The temperature measurement of each thermocouple was recorded and the results are illustrated in Figure 4–47. Thermocouple 1 was placed on the one end at the part of the embedded length and it recorded the temperature of the heated boundary. Thermocouple 2 was placed 27 mm away from the heated area. The other end on which the third thermocouple was placed was exposed to the environment.

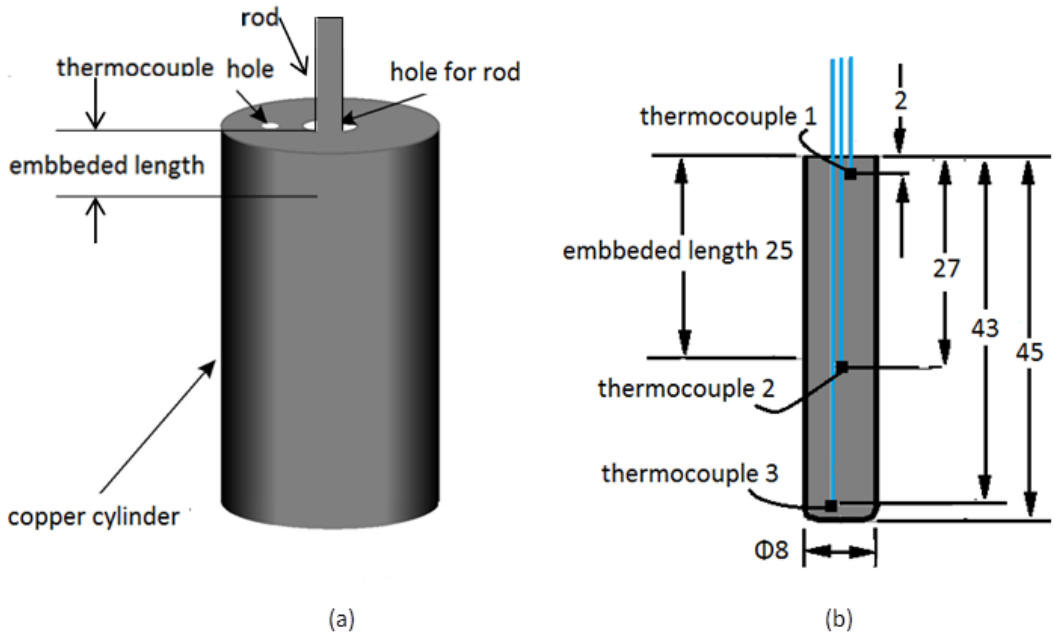

Figure 4-46 Experimental configuration. a) Copper cylinder, b) composite rod.

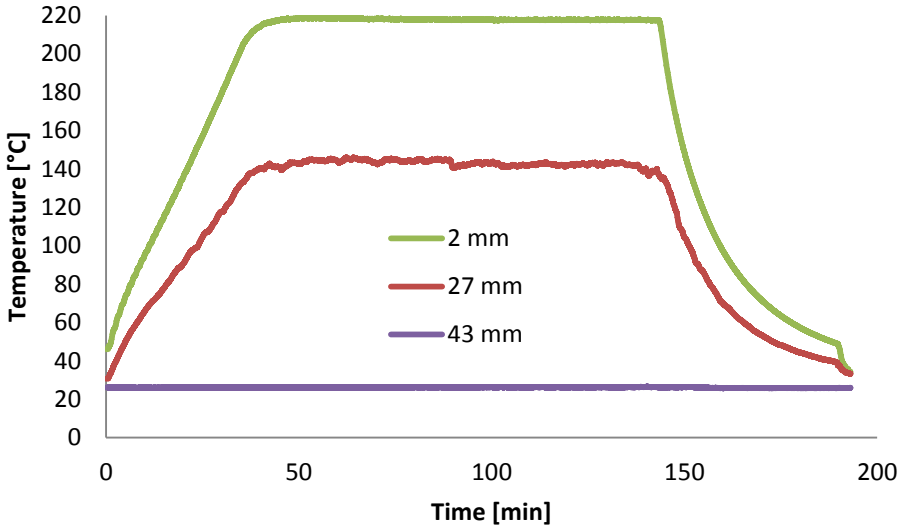

Figure 4-47 Measurements at L1=2 mm, L2=27 mm and L3=43 mm of the thermocouple 1, 2, and 3 respectively.

The electrical bulk conductivity measured at 9 different areas at ambient temperature is presented in Figure 4–48. The area close to one end which is embedded in the heating element has the highest conductivity of $2x10^{-4}$ S/m.

Moving away from this boundary the conductivity gradually decreases. At a distance of about 27 mm the temperature is 140°C which is not adequate for achieving high electrical conductivity. Over a distance of 27 mm the temperature is lower than 140°C and the material is an insulator. The grading of conductivity is evident up to a distance of 27 mm.

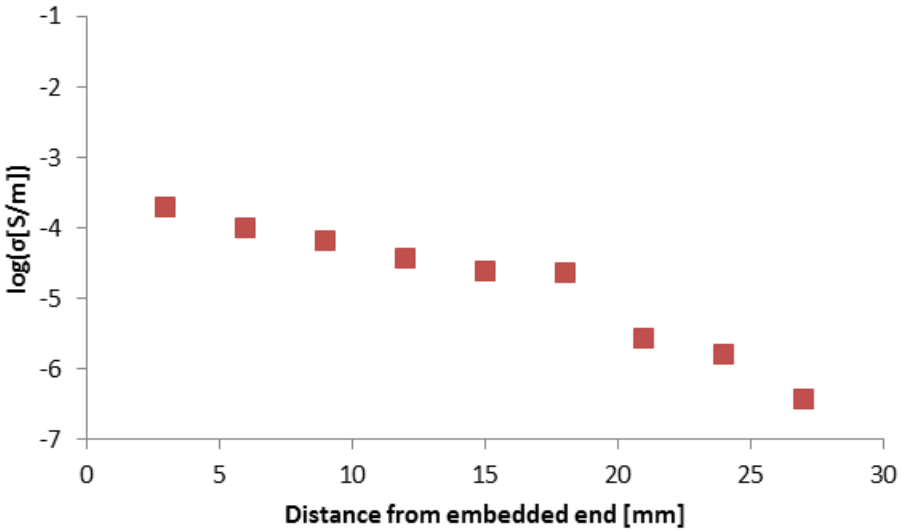

Figure 4-48 Conductivity grading of the composite rod along its length.

5 Conclusions and recommendations for further research

5.1 Conclusions

The main conclusions of this study are:

- Reduction of graphene oxide occurs at low temperatures up to 220°C. The state of thermal reduction depends on the heating rate, whereas the reaction finishes at higher temperatures in fast dynamic thermal profiles compared to the slow ones.
- The thermal reduction under isothermal conditions at high temperatures (200, 220°C) finishes within 20 minutes after reaching the dwell temperature for the dry particles.
- The total enthalpy is greater at high temperatures.
- Thermal reduction under isothermal conditions finishes within 5 minutes after reaching the dwell temperature for the composite. This means that dispersion in the epoxy accelerates reduction which occurs at lower temperatures than the dry particles.
- There are two different processes manifested in reduction under dynamic conditions.
- The composite and the particles become electrically conductive. The conductivity during heating reaches up to $7.Cx10^{-2}$ S/m for the composite and $11.5x10^{-2}$ S/m for the particle. After the treatment the material preserves its conductivity at ambient temperatures, with values of $0.9x10^{-2}$ S/m for the composite and $4x10^{-2}$ S/m for dry GO.
- Electrical measurements can be utilised to evaluate the level of reduction of the material after conventional heating and irradiation. There is clear temperature dependence of the electrical conductivity.
- The two different processes involved in reduction are evident in the evolution of electrical conductivity against temperature.
- The composite surface is electrically conductive after the application of laser irradiation on the sample. The optimisation of the laser process

parameter combination is crucial in order to obtain a conductive material and avoid resin degradation.

- ❖ During laser irradiation the local heating of the exposed area results in local reduction. As a result the conductivity can be manipulated and localised on specific areas of the material surface.
- ❖ The conductivity can also be manipulated and graded across the length of a composite rod one sided using contact heating.

5.2 Recommendations for further research

Predictive modelling can be expanded to the development of conductivity and the kinetics of reduction in the composite material. This would allow estimation of the distribution of conductivity as a function of heat transfer effects, which can lead to process design for tailored grading.

The graded conductive structure can be built using thermal treatments without altering the particle concentration at different locations. A simulation of temperature as well as conductivity distribution will lead to predictive capability that can be used in designing components with desirable conductivity distributions.

Further research for optimisation of dispersion is suggested. The study has to focus on various methods of dispersion and its evaluation through microscopy and electrical measurements until the real identification of percolation threshold. A lower percolation threshold can benefit of research on the effect of different solvents to the level of dispersion and the combination of processes. Electrical evolution can be analysed in order to determine possible dependence on the solvent.

Further characterisation can be beneficial in order to elucidate the progress of the different mechanisms of reduction. Additionally, chemically functionalised graphene derived from GO, can contribute to the determination of the mechanisms, detecting and characterising the products of chemical reactions.

REFERENCES

[1] Johnson, D. (1990), "Structure and properties of carbon fibres", in J. L. Figueiredo, C. A. Bernardo, R. T. K. Baker, K. J. Hüttinger (ed.) *Carbon Fibers Filaments and Composites,* Springer, , pp. 119-146.

[2] De Bellis, G., De Rosa, I., Dinescu, A., Sarto, M. and Tamburrano, A. (2010), "Electromagnetic absorbing nanocomposites including carbon fibers, nanotubes and graphene nanoplatelets", *Electromagnetic Compatibility (EMC), 2010 IEEE International Symposium on,* IEEE, pp. 202.

[3] Park, S. and Ruoff, R. S. (2009), "Chemical methods for the production of graphenes", *Nature Nanotechnology,* vol. 4, no. 4, pp. 217-224.

[4] Kim, K. S., Zhao, Y., Jang, H., Lee, S. Y., Kim, J. M., Kim, K. S., Ahn, J., Kim, P., Choi, J. and Hong, B. H. (2009), "Large-scale pattern growth of graphene films for stretchable transparent electrodes", *Nature,* vol. 457, no. 7230, pp. 706-710.

[5] Lu, X., Yu, M., Huang, H. and Ruoff, R. S. (1999), "Tailoring graphite with the goal of achieving single sheets", *Nanotechnology,* vol. 10, no. 3, pp. 269.

[6] Luo, J., Cote, L. J., Tung, V. C., Tan, A. T., Goins, P. E., Wu, J. and Huang, J. (2010), "Graphene oxide nanocolloids", *Journal of the American Chemical Society,* vol. 132, pp. 17667-17669.

[7] Hummers Jr, W. S. and Offeman, R. E. (1958), "Preparation of graphitic oxide", *Journal of the American Chemical Society,* vol. 80, no. 6, pp. 1339-1339.

[8] Gao, X., Jang, J. and Nagase, S. (2009), "Hydrazine and thermal reduction of graphene oxide: reaction mechanisms, product structures, and reaction design", *The Journal of Physical Chemistry C,* vol. 114, no. 2, pp. 832-842.

[9] Kim, M. C., Hwang, G. S. and Ruoff, R. S. (2009), "Epoxide reduction with hydrazine on graphene: A first principles study", *The Journal of Chemical Physics,* vol. 131, pp. 064704.

[10] Gong, C., Acik, M., Abolfath, R. M., Chabal, Y. and Cho, K. (2012), "Graphitization of Graphene Oxide with Ethanol during Thermal Reduction", *The Journal of Physical Chemistry C,* vol. 116, no. 18, pp. 9969-9979.

[11] Liu, Y., Xie, B., Zhang, Z., Zheng, Q. and Xu, Z. (2012), "Mechanical properties of graphene papers", *Journal of the Mechanics and Physics of Solids,* vol. 60, no. 4, pp. 591-605.

[12] Medhekar, N. V., Ramasubramaniam, A., Ruoff, R. S. and Shenoy, V. B. (2010), "Hydrogen bond networks in graphene oxide composite paper: structure and mechanical properties", *ACS nano,* vol. 4, no. 4, pp. 2300-2306.

[13] Dreyer, D. R., Ruoff, R. S. and Bielawski, C. W. (2010), "From conception to realization: an historial account of graphene and some perspectives for its future", *Angewandte Chemie International Edition,* vol. 49, no. 49, pp. 9336-9344.

[14] Brownson, D. A., Lacombe, A. C., Gómez-Mingot, M. and Banks, C. E. (2012), "Graphene oxide gives rise to unique and intriguing voltammetry", *RSC Advances,* vol. 2, no. 2, pp. 665-668.

[15] Lerf, A., He, H., Forster, M. and Klinowski, J. (1998), "Structure of Graphite Oxide Revisited II", *The Journal of Physical Chemistry B,* vol. 102, no. 23, pp. 4477-4482.

[16] Boukhvalov, D. W. and Katsnelson, M. I. (2008), "Modeling of graphite oxide", *Journal of the American Chemical Society,* vol. 130, no. 32, pp. 10697-10701.

[17] Yao, P., Chen, P., Jiang, L., Zhao, H., Zhu, H., Zhou, D., Hu, W., Han, B. and Liu, M. (2010), "Electric current induced reduction of graphene oxide and its application as gap electrodes in organic photoswitching devices", *Advanced Materials,* vol. 22, no. 44, pp. 5008-5012.

[18] Ramanathan, T., Abdala, A., Stankovich, S., Dikin, D., Herrera-Alonso, M., Piner, R., Adamson, D., Schniepp, H., Chen, X. and Ruoff, R. (2008), "Functionalized graphene sheets for polymer nanocomposites", *Nature Nanotechnology,* vol. 3, no. 6, pp. 327-331.

[19] Traina, M. and Pegoretti, A. (2012), "In situ reduction of graphene oxide dispersed in a polymer matrix", *Journal of Nanoparticle Research,* vol. 14, no. 4, pp. 1-6.

[20] Salavagione, H. J., Gómez, M. A. and Martínez, G. (2009), "Polymeric modification of graphene through esterification of graphite oxide and poly (vinyl alcohol)", *Macromolecules,* vol. 42, no. 17, pp. 6331-6334.

[21] Zhao, X., Zhang, Q., Chen, D. and Lu, P. (2010), "Enhanced mechanical properties of graphene-based poly (vinyl alcohol) composites", *Macromolecules,* vol. 43, no. 5, pp. 2357-2363.

[22] Pei, S. and Cheng, H. (2011), "The reduction of graphene oxide", *Carbon,* vol. 50, no. 9, pp. 3210-3228.

[23] Mao, S., Pu, H. and Chen, J. (2012), "Graphene oxide and its reduction: modeling and experimental progress", *RSC Advances,* vol. 2, no. 7, pp. 2643-2662.

[24] Mativetsky, J. M., Treossi, E., Orgiu, E., Melucci, M., Veronese, G. P., Samorì, P. and Palermo, V. (2010), "Local current mapping and patterning of reduced graphene oxide", *Journal of the American Chemical Society,* vol. 132, no. 40, pp. 14130-14136.

[25] Yin, K., Li, H., Xia, Y., Bi, H., Sun, J., Liu, Z. and Sun, L. (2011), "Thermodynamic and Kinetic Analysis of Low Temperature Thermal Reduction of Graphene Oxide", *Nano-Micro Letters,* vol. 3, no. 1, pp. 51-55.

[26] Jung, I., Field, D. A., Clark, N. J., Zhu, Y., Yang, D., Piner, R. D., Stankovich, S., Dikin, D. A., Geisler, H. and Ventrice Jr, C. A. (2009), "Reduction kinetics of graphene oxide determined by electrical transport measurements and temperature programmed desorption", *Journal of Physical Chemistry,* vol. 113, pp. 18480-18486.

[27] Acik, M., Lee, G., Mattevi, C., Chhowalla, M., Cho, K. and Chabal, Y. (2010), "Unusual infrared-absorption mechanism in thermally reduced graphene oxide", *Nature Materials,* vol. 9, no. 10, pp. 840-845.

[28] Schwamb, T., Burg, B. R., Schirmer, N. C. and Poulikakos, D. (2009), "An electrical method for the measurement of the thermal and electrical conductivity of reduced graphene oxide nanostructures", *Nanotechnology,* vol. 20, no. 40, pp. 405704.

[29] Venugopal, G., Krishnamoorthy, K., Mohan, R. and Kim, S. (2012), "An investigation of the electrical transport properties of graphene-oxide thin films", *Materials Chemistry and Physics,* vol. 132, no. 1, pp. 29-33.

[30] Punckt, C., Muckel, F., Wolff, S., Aksay, I. A., Chavarin, C. A., Bacher, G. and Mertin, W. (2013), "The effect of degree of reduction on the electrical properties of functionalized graphene sheets", *Applied Physics Letters,* vol. 102, no. 2, pp. 023114-023114-5.

[31] Wang, X., Zhi, L. and Müllen, K. (2008), "Transparent, conductive graphene electrodes for dye-sensitized solar cells", *Nano letters,* vol. 8, no. 1, pp. 323-327.

[32] Vallés, C., David Nunez, J., Benito, A. M. and Maser, W. K. (2012), "Flexible conductive graphene paper obtained by direct and gentle annealing of graphene oxide paper", *Carbon,* vol. 50, no. 3, pp. 835-844.

[33] Kim, C., Khan, W. and Park, S. (2011), "Structural evolution of graphite oxide during heat treatment", *Chemical Physics Letters,* vol. 511, no. 1, pp. 110-115.

[34] Chen, W. and Yan, L. (2010), "Preparation of graphene by a low-temperature thermal reduction at atmosphere pressure", *Nanoscale,* vol. 2, no. 4, pp. 559-563.

[35] Zhu, Y., Stoller, M. D., Cai, W., Velamakanni, A., Piner, R. D., Chen, D. and Ruoff, R. S. (2010), "Exfoliation of graphite oxide in propylene carbonate and thermal reduction of the resulting graphene oxide platelets", *ACS nano,* vol. 4, no. 2, pp. 1227-1233.

[36] Mayavan, S., Sim, J. and Choi, S. (2012), "Simultaneous reduction, exfoliation and functionalization of graphite oxide into a graphene-platinum nanoparticle hybrid for methanol oxidation", *Journal of Materials Chemistry,* vol. 22, no. 14, pp. 6953-6958.

[37] Kaniyoor, A., Baby, T. T. and Ramaprabhu, S. (2010), "Graphene synthesis via hydrogen induced low temperature exfoliation of graphite oxide", *Journal of Materials Chemistry,* vol. 20, no. 39, pp. 8467-8469.

[38] Zhang, H., Wang, J., Yan, Q., Zheng, W., Chen, C. and Yu, Z. (2011), "Vacuum-assisted synthesis of graphene from thermal exfoliation and reduction of graphite oxide", *Journal of Materials Chemistry,* vol. 21, no. 14, pp. 5392-5397.

[39] Lai, L., Chen, L., Zhan, D., Sun, L., Liu, J., Lim, S. H., Poh, C. K., Shen, Z. and Lin, J. (2011), "One-step synthesis of NH_2-graphene from in situ graphene-oxide reduction and its improved electrochemical properties", *Carbon,* vol. 49, no. 10, pp. 3250-3257.

[40] Cheng, M., Yang, R., Zhang, L., Shi, Z., Yang, W., Wang, D., Xie, G., Shi, D. and Zhang, G. (2012), "Restoration of graphene from graphene oxide by defect repair", *Carbon,* vol. 50, no. 7, pp. 2581-2587.

[41] Li, J., Lin, H., Yang, Z. and Li, J. (2011), "A method for the catalytic reduction of graphene oxide at temperatures below 150° C", *Carbon,* vol. 49, no. 9, pp. 3024-3030.

[42] Hu, H., Zhao, Z., Zhou, Q., Gogotsi, Y. and Qiu, J. (2011), "The role of microwave absorption on formation of graphene from graphite oxide", *Carbon,* vol. 50, no. 9, pp. 3267-3273.

[43] Seung Hun, H., Hye-Mi, J., Kwang Youn, C., Chang-Yeoul, K. and Eunhae, K. (2011), "Electron-beam-induced Reduction of a Graphene-oxide Film and In-situ Formation of Various Carbon Nanostructures", *Journal of Korean Physical Society,* vol. 59, pp. 3428.

[44] Shulga, Y. M., Martynenko, V., Muradyan, V., Baskakov, S., Smirnov, V. and Gutsev, G. (2010), "Gaseous products of thermo-and photo-reduction of graphite oxide", *Chemical Physics Letters,* vol. 498, no. 4, pp. 287-291.

[45] Acik, M., Guzman, R. and Chabal, Y. J. (2009), "Generation and capture of CO_2 and CO in graphite oxide stacks during thermal reduction", *MRS Proceedings,* Vol. 1205, Cambridge Univ Press, Cambridge Univ Press, .

[46] Ganguly, A., Sharma, S., Papakonstantinou, P. and Hamilton, J. (2011), "Probing the thermal deoxygenation of graphene oxide using high-resolution in situ X-ray-based spectroscopies", *The Journal of Physical Chemistry C,* vol. 115, no. 34, pp. 17009-17019.

[47] Schniepp, H. C., Li, J., McAllister, M. J., Sai, H., Herrera-Alonso, M., Adamson, D. H., Prud'homme, R. K., Car, R., Saville, D. A. and Aksay, I. A. (2006), "Functionalized single graphene sheets derived from splitting graphite oxide", *The Journal of Physical Chemistry B,* vol. 110, no. 17, pp. 8535-8539.

[48] Gao, W., Alemany, L. B., Ci, L. and Ajayan, P. M. (2009), "New insights into the structure and reduction of graphite oxide", *Nature chemistry,* vol. 1, no. 5, pp. 403-408.

[49] Acik, M., Lee, G., Mattevi, C., Pirkle, A., Wallace, R. M., Chhowalla, M., Cho, K. and Chabal, Y. (2011), "The role of oxygen during thermal reduction of graphene oxide studied by infrared absorption spectroscopy", *The Journal of Physical Chemistry C,* vol. 115, no. 40, pp. 19761-19781.

[50] McAllister, M. J., Li, J., Adamson, D. H., Schniepp, H. C., Abdala, A. A., Liu, J., Herrera-Alonso, M., Milius, D. L., Car, R. and Prud'homme, R. K. (2007), "Single sheet functionalized graphene by oxidation and thermal expansion of graphite", *Chemistry of Materials,* vol. 19, no. 18, pp. 4396-4404.

[51] Yang, D., Velamakanni, A., Bozoklu, G., Park, S., Stoller, M., Piner, R. D., Stankovich, S., Jung, I., Field, D. A. and Ventrice Jr, C. A. (2009), "Chemical analysis of graphene oxide films after heat and chemical treatments by X-ray photoelectron and micro-Raman spectroscopy", *Carbon,* vol. 47, no. 1, pp. 145-152.

[52] Chen, W., Yan, L. and Bangal, P. R. (2010), "Preparation of graphene by the rapid and mild thermal reduction of graphene oxide induced by microwaves", *Carbon,* vol. 48, no. 4, pp. 1146-1152.

[53] Nethravathi, C. and Rajamathi, M. (2008), "Chemically modified graphene sheets produced by the solvothermal reduction of colloidal dispersions of graphite oxide", *Carbon,* vol. 46, no. 14, pp. 1994-1998.

[54] Lin, Z., Yao, Y., Li, Z., Liu, Y., Li, Z. and Wong, C. (2010), "Solvent-assisted thermal reduction of graphite oxide", *The Journal of Physical Chemistry C,* vol. 114, no. 35, pp. 14819-14825.

[55] Zhou, Y., Bao, Q., Tang, L. A. L., Zhong, Y. and Loh, K. P. (2009), "Hydrothermal dehydration for the “green” reduction of exfoliated graphene oxide to graphene and demonstration of tunable optical limiting properties", *Chemistry of Materials,* vol. 21, no. 13, pp. 2950-2956.

[56] Li, Y., Gao, W., Ci, L., Wang, C. and Ajayan, P. M. (2010), "Catalytic performance of Pt nanoparticles on reduced graphene oxide for methanol electro-oxidation", *Carbon,* vol. 48, no. 4, pp. 1124-1130.

[57] Krishnan, D., Kim, F., Luo, J., Cruz-Silva, R., Cote, L. J., Jang, H. D. and Huang, J. (2012), "Energetic graphene oxide: challenges and opportunities", *Nano Today,* vol. 7, no. 2, pp. 137-152.

[58] Cote, L. J., Cruz-Silva, R. and Huang, J. (2009), "Flash reduction and patterning of graphite oxide and its polymer composite", *Journal of the American Chemical Society,* vol. 131, no. 31, pp. 11027-11032.

[59] Fatt Teoh, H., Tao, Y., Soon Tok, E., Wei Ho, G. and Haur Sow, C. (2012), "Direct laser-enabled graphene oxide–Reduced graphene oxide layered structures with micropatterning", *Journal of Applied Physics,* vol. 112, no. 6, pp. 064309-064309-6.

[60] Zhou, Y., Bao, Q., Varghese, B., Tang, L. A. L., Tan, C. K., Sow, C. and Loh, K. P. (2010), "Microstructuring of graphene oxide nanosheets using direct laser writing", *Advanced Materials,* vol. 22, no. 1, pp. 67-71.

[61] Liu, Z., Li, L., Xu, Y., Liang, J., Zhao, X., Chen, S., Chen, Y. and Tian, J. (2011), "Direct patterning on reduced graphene oxide nanosheets using femtosecond laser pulses", *Journal of Optics,* vol. 13, no. 8, pp. 085601.

[62] Sokolov, D. A., Shepperd, K. R. and Orlando, T. M. (2010), "Formation of graphene features from direct laser-induced reduction of graphite oxide", *The Journal of Physical Chemistry Letters,* vol. 1, no. 18, pp. 2633-2636.

[63] Eswaraiah, V., Aravind, S. S. J. and Ramaprabhu, S. (2011), "Top down method for synthesis of highly conducting graphene by exfoliation of graphite oxide using focused solar radiation", *Journal of Materials Chemistry,* vol. 21, no. 19, pp. 6800-6803.

[64] Guardia, L., Villar-Rodil, S., Paredes, J., Rozada, R., Martínez-Alonso, A. and Tascón, J. (2011), "UV light exposure of aqueous graphene oxide suspensions to promote their direct reduction, formation of graphene-metal nanoparticle hybrids and dye degradation", *Carbon,* .

[65] Kumar, P., Subrahmanyam, K. and Rao, C. (2011), "Graphene produced by radiation-induced reduction of graphene oxide", *International Journal of Nanoscience,* vol. 10, no. 04, pp. 559-566.

[66] Gilje, S., Dubin, S., Badakhshan, A., Farrar, J., Danczyk, S. A. and Kaner, R. B. (2010), "Photothermal Deoxygenation of Graphene Oxide for Patterning and Distributed Ignition Applications", *Advanced Materials,* vol. 22, no. 3, pp. 419-423.

[67] Trusovas, R., Ratautas, K., Račiukaitis, G., Barkauskas, J., Stankevičienė, I., Niaura, G. and Mažeikienė, R. (2012), "Reduction of graphite oxide to graphene with laser irradiation", *Carbon,* .

[68] Huang, L., Liu, Y., Ji, L., Xie, Y., Wang, T. and Shi, W. (2011), "Pulsed laser assisted reduction of graphene oxide", *Carbon,* vol. 49, no. 7, pp. 2431-2436.

[69] Potts, J. R., Dreyer, D. R., Bielawski, C. W. and Ruoff, R. S. (2011), "Graphene-based polymer nanocomposites", *Polymer,* vol. 52, no. 1, pp. 5-25.

[70] Kim, H., Abdala, A. A. and Macosko, C. W. (2010), "Graphene/polymer nanocomposites", *Macromolecules,* vol. 43, no. 16, pp. 6515-6530.

[71] Sinha Ray, S. and Okamoto, M. (2003), "Polymer/layered silicate nanocomposites: a review from preparation to processing", *Progress in polymer science,* vol. 28, no. 11, pp. 1539-1641.

[72] Tang, H., Ehlert, G. J., Lin, Y. and Sodano, H. A. (2011), "Highly efficient synthesis of graphene nanocomposites", *Nano letters,* vol. 12, no. 1, pp. 84-90.

[73] Wei, T., Luo, G., Fan, Z., Zheng, C., Yan, J., Yao, C., Li, W. and Zhang, C. (2009), "Preparation of graphene nanosheet/polymer composites using in situ reduction–extractive dispersion", *Carbon,* vol. 47, no. 9, pp. 2296-2299.

[74] Kim, H., Miura, Y. and Macosko, C. W. (2010), "Graphene/polyurethane nanocomposites for improved gas barrier and electrical conductivity", *Chemistry of Materials,* vol. 22, no. 11, pp. 3441-3450.

[75] Cao, Y., Lai, Z., Feng, J. and Wu, P. (2011), "Graphene oxide sheets covalently functionalized with block copolymers via click chemistry as reinforcing fillers", *Journal of Materials Chemistry,* vol. 21, no. 25, pp. 9271-9278.

[76] Yang, H., Shan, C., Li, F., Zhang, Q., Han, D. and Niu, L. (2009), "Convenient preparation of tunably loaded chemically converted graphene

oxide/epoxy resin nanocomposites from graphene oxide sheets through two-phase extraction", *Journal of Materials Chemistry,* vol. 19, no. 46, pp. 8856-8860.

[77] Huang, Y., Qin, Y., Zhou, Y., Niu, H., Yu, Z. and Dong, J. (2010), "Polypropylene/Graphene oxide nanocomposites prepared by in situ Ziegler− Natta polymerization", *Chemistry of Materials,* vol. 22, no. 13, pp. 4096-4102.

[78] Lee, S. H., Dreyer, D. R., An, J., Velamakanni, A., Piner, R. D., Park, S., Zhu, Y., Kim, S. O., Bielawski, C. W. and Ruoff, R. S. (2010), "Polymer Brushes via Controlled, Surface-Initiated Atom Transfer Radical Polymerization (ATRP) from Graphene Oxide", *Macromolecular rapid communications,* vol. 31, no. 3, pp. 281-288.

[79] Shen, J., Hu, Y., Li, C., Qin, C. and Ye, M. (2009), "Synthesis of amphiphilic graphene nanoplatelets", *small,* vol. 5, no. 1, pp. 82-85.

[80] Fang, M., Wang, K., Lu, H., Yang, Y. and Nutt, S. (2009), "Covalent polymer functionalization of graphene nanosheets and mechanical properties of composites", *Journal of Materials Chemistry,* vol. 19, no. 38, pp. 7098-7105.

[81] Xu, C., Gao, J., Xiu, H., Li, X., Zhang, J., Luo, F., Zhang, Q., Chen, F. and Fu, Q. (2013), "Can in situ thermal reduction be a green and efficient way in the fabrication of electrically conductive polymer/reduced graphene oxide nanocomposites?", *Composites Part A: Applied Science and Manufacturing,* vol. 53, no. 0, pp. 24-33.

[82] Baughman, R. H., Zakhidov, A. A. and de Heer, W. A. (2002), "Carbon nanotubes--the route toward applications", *Science,* vol. 297, no. 5582, pp. 787-792.

[83] Du, J., Bai, J. and Cheng, H. (2007), "The present status and key problems of carbon nanotube based polymer composites", *Express Polymer Letters,* vol. 1, no. 5, pp. 253-273.

[84] Sharif, F. and Gudarzi, M. M. (2012), "Enhancement of dispersion and bonding of graphene-polymer through wet transfer of functionalized graphene oxide", *eXPRESS Polymer Letters,* vol. 6.

[85] Qiu, S., Wang, C., Wang, Y., Liu, C., Chen, X., Xie, H., Huang, Y. and Cheng, R. (2011), "Effects of graphene oxides on the cure behaviors of a tetrafunctional epoxy resin", *Express Polymer Letters,* vol. 5, pp. 809-818.

[86] Lu, K., Lago, R., Chen, Y., Green, M., Harris, P. and Tsang, S. (1996), "Mechanical damage of carbon nanotubes by ultrasound", *Carbon,* vol. 34, no. 6, pp. 814-816.

[87] Kuilla, T., Bhadra, S., Yao, D., Kim, N. H., Bose, S. and Lee, J. H. (2010), "Recent advances in graphene based polymer composites", *Progress in Polymer Science,* vol. 35, no. 11, pp. 1350-1375.

[88] Jiang, T., Kuila, T., Kim, N. H., Ku, B. and Lee, J. H. (2013), "Enhanced mechanical properties of silanized silica nanoparticle attached graphene oxide/epoxy composites", *Composites Science and Technology,* .

[89] Park, S., An, J., Jung, I., Piner, R. D., An, S. J., Li, X., Velamakanni, A. and Ruoff, R. S. (2009), "Colloidal suspensions of highly reduced graphene oxide in a wide variety of organic solvents", *Nano Letters,* vol. 9, no. 4, pp. 1593-1597.

[90] Glover, A. J., Cai, M., Overdeep, K. R., Kranbuehl, D. E. and Schniepp, H. C. (2011), "In Situ Reduction of Graphene Oxide in Polymers", *Macromolecules,* vol. 44, no. 24, pp. 9821-9829.

[91] Blake, P., Brimicombe, P. D., Nair, R. R., Booth, T. J., Jiang, D., Schedin, F., Ponomarenko, L. A., Morozov, S. V., Gleeson, H. F. and Hill, E. W. (2008), "Graphene-based liquid crystal device", *Nano letters,* vol. 8, no. 6, pp. 1704-1708.

[92] Fei Liu, Ruimei Huo, Xingyi Huang, Pingkai Jiang (2013), "Effect of Processing Method on the Dielectric Behavior of Graphene Oxide/PVDF Nanocomposites", *2013 IEEE International Conference on Solid Dielectrics (ICSD),* June 30-July 4 2013, Bologna, pp. 919.

[93] Pham, V. H., Cuong, T. V., Hur, S. H., Oh, E., Kim, E. J., Shin, E. W. and Chung, J. S. (2010), "Chemical functionalization of graphene sheets by solvothermal reduction of a graphene oxide suspension in N-methyl-2-pyrrolidone", *Journal of Materials Chemistry,* vol. 21, no. 10, pp. 3371-3377.

[94] Dubin, S., Gilje, S., Wang, K., Tung, V. C., Cha, K., Hall, A. S., Farrar, J., Varshneya, R., Yang, Y. and Kaner, R. B. (2010), "A one-step, solvothermal reduction method for producing reduced graphene oxide dispersions in organic solvents", *ACS nano,* vol. 4, no. 7, pp. 3845-3852.

[95] Hernandez, Y., Nicolosi, V., Lotya, M., Blighe, F. M., Sun, Z., De, S., McGovern, I., Holland, B., Byrne, M. and Gun'Ko, Y. K. (2008), "High-yield production of graphene by liquid-phase exfoliation of graphite", *Nature Nanotechnology,* vol. 3, no. 9, pp. 563-568.

[96] Gudarzi, M. M. and Sharif, F. (2010), "Characteristics of polymers that stabilize colloids for the production of graphene from graphene oxide", *Journal of colloid and interface science,* vol. 349, no. 1, pp. 63-69.

[97] Liang, J., Huang, Y., Zhang, L., Wang, Y., Ma, Y., Guo, T. and Chen, Y. (2009), "Molecular-Level Dispersion of Graphene into Poly (vinyl alcohol)

and Effective Reinforcement of their Nanocomposites", *Advanced Functional Materials,* vol. 19, no. 14, pp. 2297-2302.

[98] Gudarzi, M. M. and Sharif, F. (2011), "Molecular level dispersion of graphene in polymer matrices using colloidal polymer and graphene", *Journal of colloid and interface science,* vol. 19, no. 14, pp. 2297-2302.

[99] Jiang, L., Shen, X., Wu, J. and Shen, K. (2010), "Preparation and characterization of graphene/poly (vinyl alcohol) nanocomposites", *Journal of Applied Polymer Science,* vol. 118, no. 1, pp. 275-279.

[100] Fang, M., Zhang, Z., Li, J., Zhang, H., Lu, H. and Yang, Y. (2010), "Constructing hierarchically structured interphases for strong and tough epoxy nanocomposites by amine-rich graphene surfaces", *Journal of Materials Chemistry,* vol. 20, no. 43, pp. 9635-9643.

[101] An, X., Simmons, T., Shah, R., Wolfe, C., Lewis, K. M., Washington, M., Nayak, S. K., Talapatra, S. and Kar, S. (2010), "Stable aqueous dispersions of noncovalently functionalized graphene from graphite and their multifunctional high-performance applications", *Nano letters,* vol. 10, no. 11, pp. 4295-4301.

[102] Ansari, S. and Giannelis, E. P. (2009), "Functionalized graphene sheet—Poly (vinylidene fluoride) conductive nanocomposites", *Journal of Polymer Science Part B: Polymer Physics,* vol. 47, no. 9, pp. 888-897.

[103] Wang, Z., Nelson, J. K., Hillborg, H., Zhao, S. and Schadler, L. S. (2012), "Graphene oxide filled nanocomposite with novel electrical and dielectric properties", *Advanced Materials,* vol. 24, no. 23, pp. 3134-3137.

[104] Zheng, D., Tang, G., Zhang, H., Yu, Z., Yavari, F., Koratkar, N., Lim, S. and Lee, M. (2011), "In-situ thermal reduction of graphene oxide for high electrical conductivity and low percolation threshold in polyamide 6 nanocomposites", *Composites Science and Technology,* .

[105] Shen, Y., Jing, T., Ren, W., Zhang, J., Jiang, Z., Yu, Z. and Dasari, A. (2012), "Chemical and thermal reduction of graphene oxide and its electrically conductive polylactic acid nanocomposites", *Composites Science and Technology,* vol. 72, no. 12, pp. 1430-1435.

[106] Xu, Z. and Gao, C. (2010), "In situ polymerization approach to graphene-reinforced nylon-6 composites", *Macromolecules,* vol. 43, no. 16, pp. 6716-6723.

[107] Fabbri, P., Valentini, L., Bon, S. B., Foix, D., Pasquali, L., Montecchi, M. and Sangermano, M. (2012), "In-situ graphene oxide reduction during UV-photopolymerization of graphene oxide/acrylic resins mixtures", *Polymer,* .

[108] Aldosari, M. A., Othman, A. A. and Alsharaeh, E. H. (2013), "Synthesis and Characterization of the in Situ Bulk Polymerization of PMMA Containing Graphene Sheets Using Microwave Irradiation", *Molecules,* vol. 18, no. 3, pp. 3152-3167.

[109] Mancinelli P, Fabiani D, Saccani A, Tosseli M, Heid T, Frechette M, Savoie S, David E (2013), "Preparation and dielectric behaviour of epoxy resin containing graphene oxide", ***11th IEEE International Conference on Solid Dielectrics****,* 04/Jul/2013, Bologna, .

[110] Liang, J., Wang, Y., Huang, Y., Ma, Y., Liu, Z., Cai, J., Zhang, C., Gao, H. and Chen, Y. (2009), "Electromagnetic interference shielding of graphene/epoxy composites", *Carbon,* vol. 47, no. 3, pp. 922-925.

[111] Galpaya, D., Wang, M., Liu, M., Motta, N., Waclawik, E. R. and Yan, C. (2012), "Recent advances in fabrication and characterization of graphene-polymer nanocomposites", *Graphene,* vol. 1, no. 2, pp. 30-49.

[112] Ma, H., Zhang, H., Hu, Q., Li, W., Jiang, Z., Yu, Z. and Dasari, A. (2012), "Functionalization and reduction of graphene oxide with p-phenylene diamine for electrically conductive and thermally stable polystyrene composites", *ACS Applied Materials & Interfaces,* vol. 4, no. 4, pp. 1948-1953.

[113] Park, O., Hahm, M. G., Lee, S., Joh, H., Na, S., Vajtai, R., Lee, J. H., Ku, B. and Ajayan, P. M. (2012), "In Situ Synthesis of Thermochemically Reduced Graphene Oxide Conducting Nanocomposites", *Nano letters,* vol. 12, no. 4, pp. 1789-1793.

[114] Ansari, S., Kelarakis, A., Estevez, L. and Giannelis, E. P. (2010), "Oriented arrays of graphene in a polymer matrix by in situ reduction of graphite oxide nanosheets", *Small,* vol. 6, no. 2, pp. 205-209.

[115] Huntsman (2003)*, Araldite CY 221, HY 2967*, available at: http://www.chemcenters.com/images/suppliers/169257/Araldite%20CY%20221,%20HY%202967.pdf (accessed 12/10).

[116] NanoInnova *, Graphene Oxide Characterization sheet*, available at: http://www.nanoinnova.com/Uploads/Features/5774308.pdf (accessed 12/11).

[117] Graphene Laboratories *, Grephene Oxide Paper*, available at: https://graphene-supermarket.com/Graphene-Oxide-Paper.html (accessed 01/26).

[118] Pearson Panke Ltd *, Pearson Panke Engineering solutions*, available at: http://www.pearsonpanke.co.uk/ (accessed 01/26).

[119] Karkanas, P. I. (1998), *Cure modelling and monitoring of epoxy/amine resin systems,* Ph.D. Thesis, Cranfield University, Cranfield.

[120] Kazilas, M. C. (2003), *Acquisition and interpretation of dielectric data for thermoset cure monitoring,* Ph.D. Thesis, Cranfield University, Cranfield.

[121] Moussa, S., Abdelsayed, V. and Samy El-Shall, M. (2011), "Laser synthesis of Pt, Pd, CoO and Pd–CoO nanoparticle catalysts supported on graphene", *Chemical Physics Letters,* vol. 510, no. 4, pp. 179-184.

[122] Bilyeu, B., Brostow, W. and Menard, K. P. (2001), "Epoxy thermosets and their applications. III. Kinetic equations and models", *J.Mater.Ed,* vol. 23, pp. 189-197.

[123] M. Gougis (2000), Graphite nanoplatelets/epoxy nanocomposites, Thesis, Cranfield University, Cranfield.